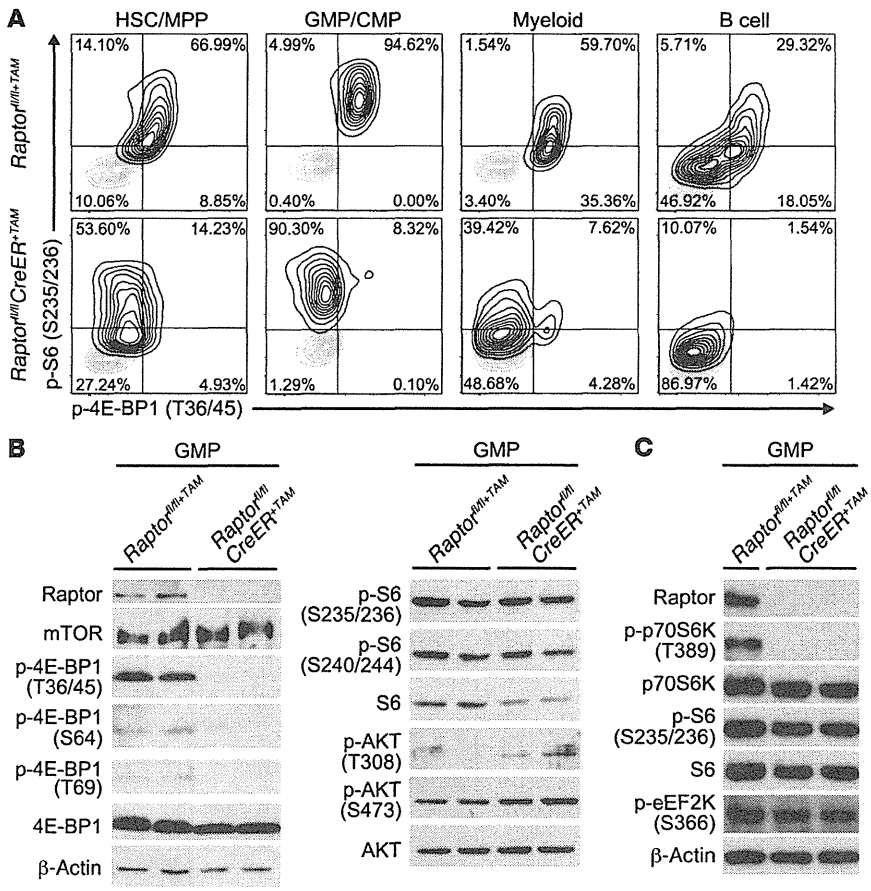

Figure 3
Deletion of *Raptor* has differential effects on phosphorylation of mTORC1 effectors in different hematopoietic cell contexts. (**A**) Flow cytometric analysis of intracellular p-S6 and p–4E-BP1. Data shown are levels of p-S6 (S235/236) and p–4E-BP1 (T36/45) in the indicated BM MNC subpopulations from control and *Raptor*-deficient mice. Cells were collected 10 days after the last injection of TAM. (**B**) Phosphorylation of mTOR signaling pathway proteins in GMPs. Lysates of GMPs isolated from control and *Raptor*-deficient mice were immunoblotted to detect the indicated proteins. β-Actin was used as loading control. Results are representative of at least 3 independent trials. (**C**) Phosphorylation of p70S6K and its substrates in GMPs. Lysates of GMPs isolated from control and *Raptor*-deficient mice were immunoblotted to detect the indicated proteins. β-Actin was used as loading control. Results are representative of at least 3 independent trials.

lation in all hematopoietic cell populations. Unexpectedly, however, S6 phosphorylation was not inhibited in GMPs and CMPs. In contrast, S6 phosphorylation was markedly downregulated in *Raptor*-deficient B220$^+$ B cells.

To confirm these findings biochemically, we performed immunoblotting analyses of GMPs. Consistent with our flow cytometric analyses, phosphorylation of S6 (at S235/236 and S240/244) was not altered by *Raptor* deficiency (Figure 3B). In contrast, 4E-BP1 phosphorylation at all 4 sites, T36/45, S64, and T69, was strongly inhibited in the absence of Raptor. The phosphorylation of p70S6K, a direct target of mTORC1, was also dramatically inhibited by Raptor deficiency, whereas phosphorylation of eEF2K, a target molecule of p70S6K, was not affected in GMPs (Figure 3C), suggesting that S6 and eEF2K are phosphorylated in an mTOR-independent manner, as previously reported (28–30). Thus, these results indicate that the phosphorylation of downstream molecules in the mTORC1 pathway is highly variable among hematopoietic lineages.

Raptor deficiency suppresses AML progression in vivo. To evaluate the role of mTORC1 in established AML, we investigated the effects of mTORC1 inactivation via genetic ablation of *Raptor* in a murine AML model. To create a representative AML model, we first inserted the *MLL-AF9* fusion gene (17, 18, 21) into K$^+$S$^+$L$^-$ cells isolated from *Raptor*$^{fl/fl}$, *Raptor*$^{+/+}$*CreER*, or *Raptor*$^{fl/fl}$*CreER* mice by using retrovirus-mediated transfer. We then transplanted these genetically modified cells into lethally irradiated syngeneic recipients to generate *Raptor*$^{fl/fl}$, *Raptor*$^{+/+}$*CreER*, and *Raptor*$^{fl/fl}$*CreER* AML mice, respectively (Figure 4A). In the absence of TAM treatment, all 3 sets of recipient mice soon developed AML characterized by a significant increase in GFP$^+$Mac-1$^+$ leukemic cells in spleen and BM (Supplemental Figure 6). To determine the effect of mTORC1 inactivation on AML in vivo, we carried out a second transplantation in which BM-MNCs from AML mice were transferred into fresh recipients (along with WT rescue cells). We administered TAM to these animals to delete *Raptor* and monitored their survival and AML progression. TAM injection significantly prolonged the survival of the *Raptor*$^{fl/fl}$*CreER* AML mice, but not that of *Raptor*$^{fl/fl}$ AML mice (Figure 4, B and C) or *Raptor*$^{+/+}$*CreER* AML mice (Supplemental Figure 7). These data indicate that the prolonged life span of the *Raptor*$^{fl/fl}$*CreER* AML mice treated with TAM was due to *Raptor* deficiency and not Cre toxicity (Supplemental Figure 7A).

Although all *Raptor*$^{fl/fl}$*CreER*$^{+TAM}$ (*Raptor*-deficient) AML mice died by 42 days post-TAM, the reason for the deaths was the progression of AML cells with incomplete deletion of the *Raptor* gene. Therefore, we analyzed the characteristics of the AML cells at 14 days post-TAM, because we found efficient deletion of the *Raptor* gene in all *Raptor*$^{fl/fl}$*CreER*$^{+TAM}$ AML mice at this time point. Consistent with their prolonged survival, the number of wbc in the PB of *Raptor*$^{fl/fl}$*CreER*$^{+TAM}$ AML mice at 14 days post-TAM injection decreased dramatically compared with that in control *Raptor*$^{fl/fl}$ *CreER*$^{-TAM}$ AML mice (Figure 4D). Previous reports on this AML model have indicated that c-Kit marks undifferentiated AML cells (17, 18, 31). In the PB of our control AML mice, most AML cells (GFP$^+$) did not express c-Kit (Figure 4E), indicating that AML cells

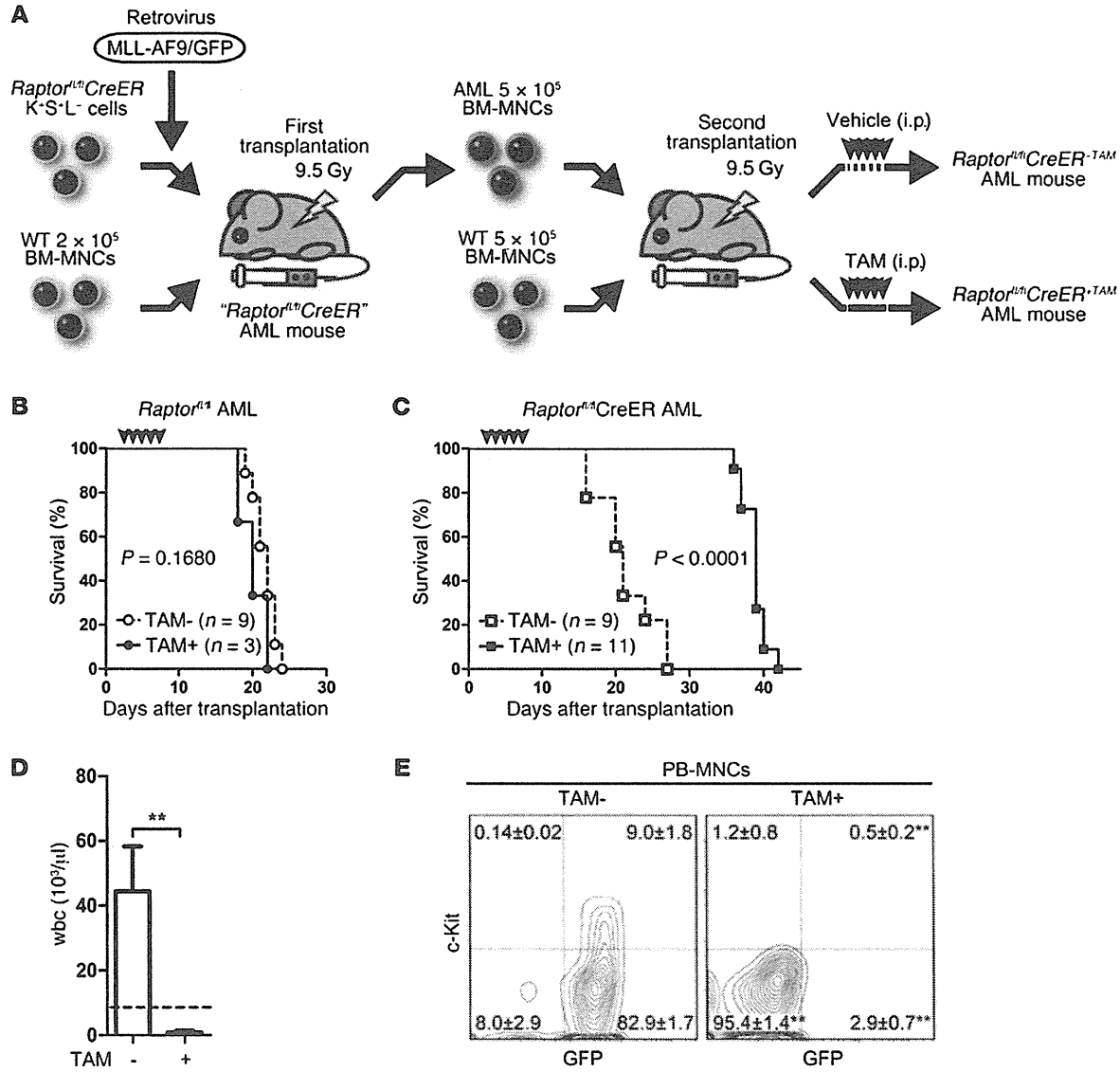

Figure 4

Generation of a *Raptor*-deficient murine AML model. (**A**) Experimental design for a *Raptor*-deficient murine AML model. (**B** and **C**) Survival of AML mice. *Raptor*$^{fl/fl}$ AML mice (**B**) and *Raptor*$^{fl/fl}$*CreER* AML mice (**C**) were established as illustrated in **A**. BM-MNCs from these animals were transplanted into a fresh set of recipients (along with rescue cells), and these animals were treated with oil diluent as the control (TAM–) or with TAM (TAM+) to generate the indicated control and *Raptor*-deficient AML mice. *P* value were determined by the log-rank test. (**D**) Number of wbc in PB. PB samples were obtained from the *Raptor*$^{fl/fl}$*CreER* AML mice at 14 days after control or TAM treatment. Data shown are mean number ± SD (TAM–, $n = 6$; TAM+ $n = 9$). The horizontal dotted line is the mean value of the number of wbc in normal adult mice (8 weeks old, $n = 5$). (**E**) Flow cytometric analyses of AML cells in PB. PB samples were obtained from the *Raptor*$^{fl/fl}$*CreER* AML mice at 14 days after control or TAM treatment. Representative data are shown for GFP/c-Kit expression in PB-MNCs. Values in panels are the mean percentage ± SD for the indicated subpopulations ($n = 4$). $^{**}P < 0.01$ (Student's *t* test).

present in the circulation had differentiated. Upon TAM injection, AML cells disappeared from the PB of *Raptor*$^{fl/fl}$*CreER*$^{+TAM}$ AML mice (Figure 4E), but not of *Raptor*$^{+/+}$*CreER*$^{+TAM}$ AML mice (Supplemental Figure 7B). Pharmaceutical inhibition of mTORC1 by rapamycin slightly prolonged the survival of AML mice, but it had a milder effect than *Raptor* deficiency (Supplemental Figure 8, A and B). Thus, *Raptor* deficiency significantly suppressed AML progression in vivo, thereby prolonging the life span of AML mice.

mTORC1 inactivation induces dramatic levels of apoptosis in differentiated, but not undifferentiated, AML cells. Next, we investigated the effect of *Raptor* deficiency on AML cells in BM. Interestingly, the reduction in the number of AML cells in the BM of *Raptor*$^{fl/fl}$*CreER*$^{+TAM}$ AML mice was much milder than that observed in the PB of the same animals (Figure 5, A and C). In addition, platelet counts were not restored to normal in mutant AML mice (Figure 5B). These data suggest that *Raptor* deficiency did not rescue the

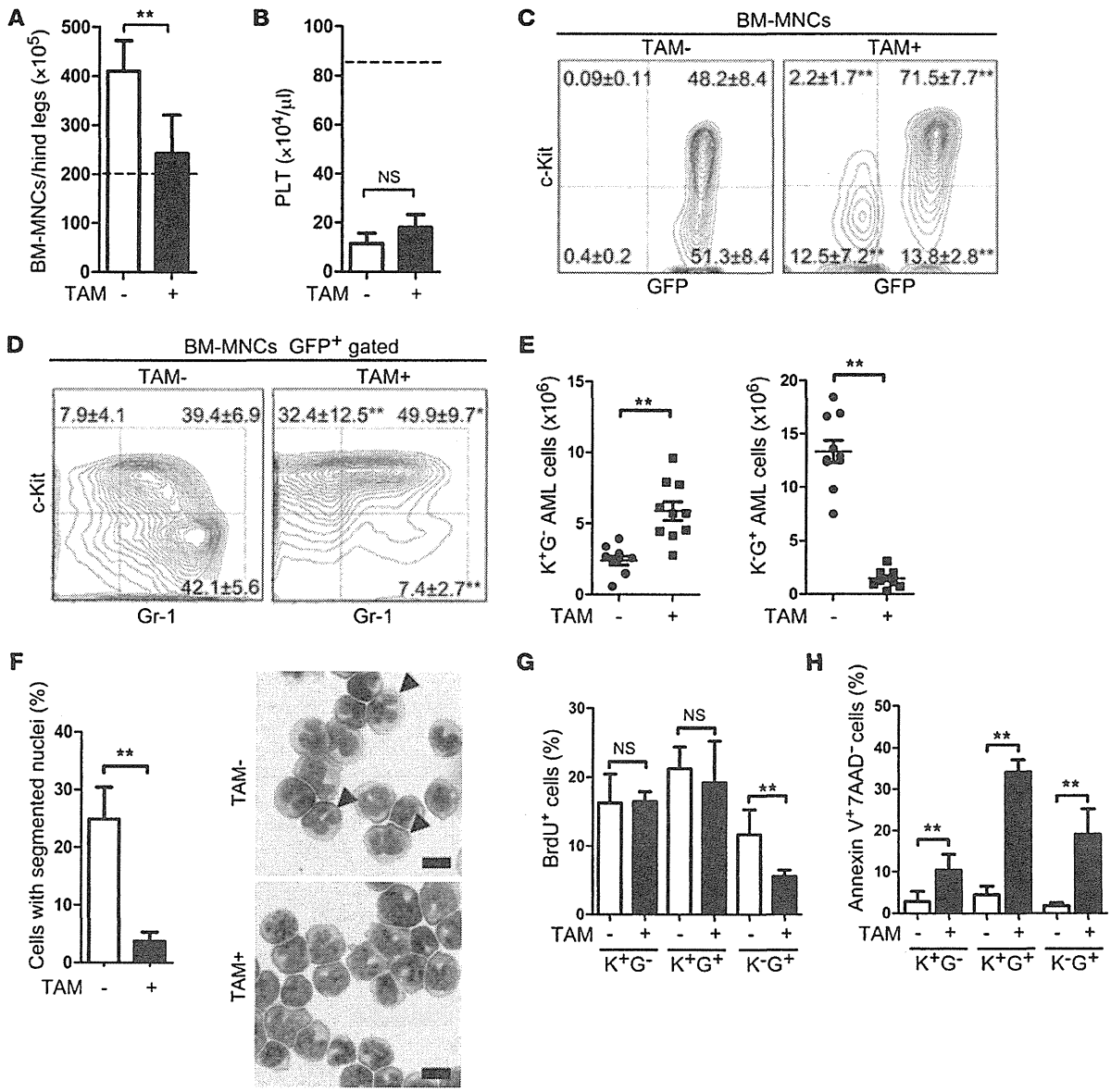

Figure 5

Undifferentiated AML cells are resistant to loss of mTORC1 activity. The *Raptor*$^{fl/fl}$*CreER* AML mice were analyzed 14 days after control or TAM treatment. (**A** and **B**) Number of BM-MNCs in BM (**A**: TAM–, $n = 6$; TAM+, $n = 5$) and of platelets (PLT) in PB (**B**: TAM–, $n = 6$; TAM+, $n = 9$). Data are mean number ± SD of the indicated hematopoietic cell type. Horizontal dotted lines are mean values of the indicated hematopoietic parameters in normal adult mice (8 weeks old, $n = 5$). (**C** and **D**) Flow cytometric analyses of AML cells in BM. Representative data are shown for GFP/c-Kit expression in BM-MNCs (**C**) and for c-Kit/Gr-1 expression in GFP$^+$-gated BM-MNCs (**D**). Values are the mean percentage ± SD for the indicated subpopulations (**C**, $n = 10$; **D**, $n = 3$). (**E**) Absolute numbers of K^+G^- and K^-G^+ cells in the hind legs of the *Raptor*$^{fl/fl}$*CreER* AML mice (TAM– or TAM+). Data shown are the values for individual mice ($n = 10$ per group). Horizontal lines are mean values. (**F**) Morphological analysis of AML cells. GFP$^+$ cells from the BM of AML mice were stained with May-Grünwald/Giemsa. Data are the mean percentage ± SD of AML cells containing segmented nuclei ($n = 5$). Right panels show representative images of GFP$^+$ cells. Scale bars: 10 μm. Arrowheads indicate AML cells with segmented nuclei (differentiated AML cells). (**G**) Cell cycle. BrdU was injected i.p. into AML mice 2 hours prior to sacrifice. AML cells were harvested, stained with an anti-BrdU Ab, and analyzed by flow cytometry. Data are the mean percentage ± SD of BrdU$^+$ cells in the indicated AML cell subpopulations ($n = 5$). (**H**) Apoptosis. Data shown are the mean percentage ± SD of Annexin V$^+$7AAD$^-$ cells in the indicated AML cell subpopulations ($n = 5$). $^*P < 0.05$, $^{**}P < 0.01$ (Student's *t* test).

hematopoietic failure seen in AML mice due to the occupation of the BM by AML cells.

To evaluate the properties of AML cells in the BM of *Raptor*$^{fl/fl}$ *CreER*$^{+TAM}$ AML mice, we analyzed expression of cell surface markers at various stages of AML cell differentiation. Previous reports on this AML model have shown that AML stem cells are highly enriched in the c-Kit$^+$Gr-1$^-$ (K^+G^-) population (31). Upon TAM injection, c-Kit$^+$ AML cells were enriched in the BM of *Raptor*$^{fl/fl}$

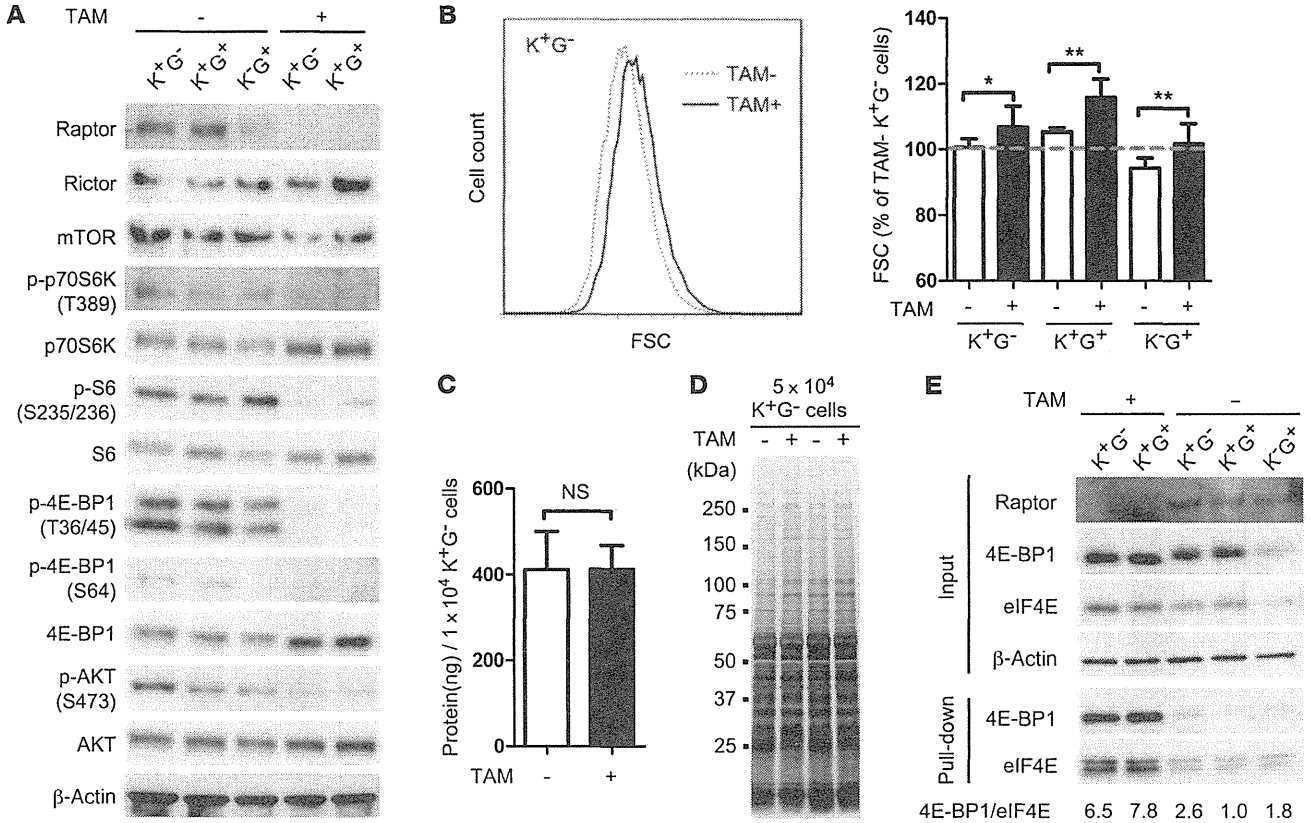

Figure 6

4E-BP1–independent cell growth of *Raptor*-deficient AML cells. (**A**) Phosphorylation of mTOR signaling pathway proteins. Lysates were prepared from the indicated AML cell subpopulations and immunoblotted to detect the indicated proteins. (**B**) Flow cytometric analysis of cell size. Left: Representative histogram shows forward scatter (FSC) of K^+G^- AML cells from the mice in **A**. Right: Quantification. All FSC values were normalized to the mean value (dotted line) obtained for K^+G^- AML cells from control AML mice in 10 independent experiments. Data shown are mean normalized FSC values ± SD (n = 10). (**C** and **D**) Amount of protein in K^+G^- AML cells. Lysates were prepared from K^+G^- AML cells 14 days post-TAM. Proteins were quantified with a BCA protein assay (**C**), and SDS-PAGE was performed, followed by silver staining, to visualize protein levels (**D**). Data in **C** are the mean ± SD of the amount of protein (ng) in 1 × 10^4 K^+G^- AML cells (n = 8). (**E**) 7-methyl GTP pull-down assay. Lysates were prepared from the indicated AML cell subpopulations, incubated with 7-methyl GTP-Sepharose beads, washed, and immunoblotted to detect the indicated proteins. Numbers below the panel are the ratios of the intensity of the 4E-BP1 and eIF4E protein band signals. $^*P < 0.05$, $^{**}P < 0.01$ (Student's t test).

CreER AML mice (Figure 5C), but not *Raptor*$^{+/+}$*CreER* AML mice (Supplemental Figure 7, D and E). In addition, *Raptor* deficiency increased the proportion of K^+G^- cells, whereas the proportion of K^-G^+ cells decreased (Figure 5D). The absolute number of K^-G^+ AML cells dropped precipitously upon deletion of *Raptor*, whereas that of K^+G^- AML cells increased (Figure 5E). Morphological analysis of AML cells confirmed that *Raptor* deficiency was associated with decreased differentiation, as judged by the lack of cells with segmented nuclei (Figure 5F). These data suggest that differentiated AML cells, but not undifferentiated AML cells, require mTORC1 for survival or proliferation. In vivo BrdU incorporation studies showed that loss of *Raptor* resulted in a decrease in proliferation of K^-G^+ AML cells, but it had no effect on either K^+G^+ or K^+G^- AML cells (Figure 5G). In contrast, apoptosis was increased by *Raptor* deficiency in all AML cell populations examined but was most highly elevated in K^+G^+ AML cells (Figure 5H). No significant effect on apoptosis was seen in these cell populations from control *Raptor*$^{+/+}$*CreER* AML mice (Supplemental Figure 7F). These data indicate that the loss of differentiated AML cells following mTORC1 inactivation is due to both increased apoptosis and decreased cell proliferation, whereas undifferentiated (K^+G^-) AML cells are enriched because of reduced apoptosis.

4E-BP1–independent cell growth of AML cells. To examine the molecular changes occurring in AML cells lacking mTORC1 activity, we carried out immunoblotting analyses. The phosphorylation of p70S6K, 4E-BP1, and S6 was dramatically suppressed in *Raptor*-deficient, but not control, AML cells, including the AML stem cell population (K^+G^- cells), indicating downregulated mTORC1 activity (Figure 6A and Supplemental Figure 7G). Rapamycin treatment effectively suppressed the phosphorylation of p70S6K and S6 in AML cells, whereas it did not affect phosphorylation of 4E-BP1 (Supplemental Figure 8C). A similar phenomenon was observed in embryonic fibroblasts (Supplemental Figure 1E), which is consistent with previous reports showing that 4E-BP1 is a rapamycin-insensitive mTORC1 target (24, 25). Although it has been reported that mTORC1 inactivation leads to enhanced AKT phosphorylation in some cell types

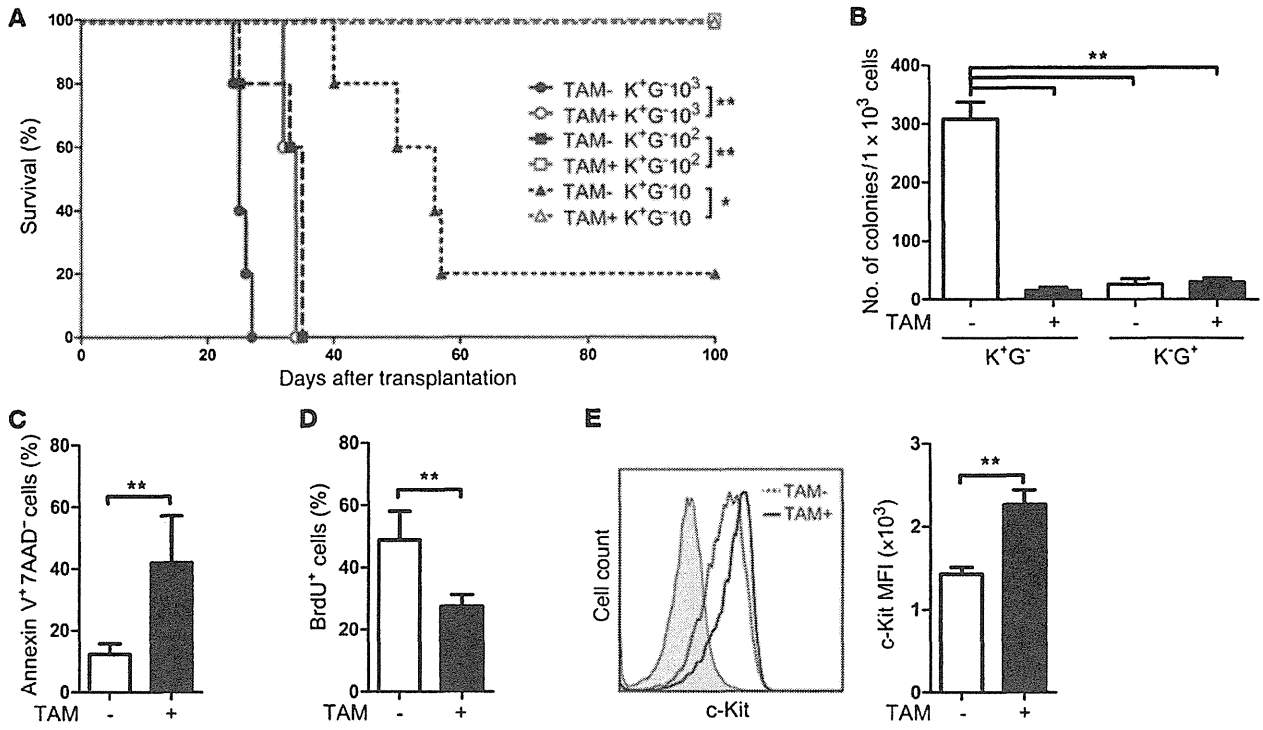

Figure 7

Raptor-deficient AML stem cells show defective leukemia-initiating capacity. (**A**) Limiting dilution transplantation assay. The indicated numbers of K^+G^- AML cells from the mice 14 days after control or TAM treatment were transplanted into lethally irradiated recipients along with WT BM-MNCs (rescue cells), and survival was monitored (n = 5/group). $^*P < 0.05$, $^{**}P < 0.01$ (log-rank test). (**B**) Colony-forming ability of AML cells. K^-G^+ and K^+G^- AML cells were isolated from *Raptor*$^{fl/fl}$*CreER* AML mice 14 days after control or TAM treatment and cultured in semisolid medium for 7 days. Data are the mean colony numbers ± SD (n = 3). (**C**) Apoptosis of K^+G^- AML cells after 12 hours of stimulation with the cytokines SCF, IL-3, and IL-6. Data shown are the mean percentage ± SD of Annexin V^+7AAD^- cells (n = 8). (**D**) Cell cycle of K^+G^- AML cells after 12 hours of stimulation with the same set of cytokines. Data shown are the mean percentage ± SD of $BrdU^+$ cells (n = 8). (**E**) Expression level of c-Kit on K^+G^- AML cells after 12 hours of cytokine stimulation. Representative histograms are shown in the left panel. Shaded histogram: nonstained AML cells; dotted line: *Raptor*$^{fl/fl}$*CreER*$^{-TAM}$ AML cells; solid line: *Raptor*$^{fl/fl}$*CreER*$^{+TAM}$ AML cells. Data in the right panel are the mean percentage ± SD of MFI of c-Kit (n = 3). For **B**–**E**, $^{**}P < 0.01$ (Student's t test).

(32, 33), neither *Raptor* deficiency nor rapamycin resulted in hyperphosphorylation of AKT (S473) (Figure 6A and Supplemental Figure 8D). These data suggest that the feedback loop for AKT inhibition through mTORC1 might not occur in these AML cells.

Although mTORC1 reportedly controls cell size (cell growth) (34), we did not observe a decrease in the size of our *Raptor*-deficient AML cells (Figure 6B), and we found that the amount of protein per cell was comparable in control and *Raptor*-deficient AML stem cells (Figure 6, C and D). Inactivation of mTORC1 is also reported to suppress cap-dependent protein translation by enhancing binding between 4E-BP1 and eIF4E (35, 36). Consistent with this, the hypophosphorylation of 4E-BP1 induced by *Raptor* deficiency enhanced binding of 4E-BP1 to eIF4E, which binds the 7-methyl-guanosine cap structure, as determined by a 7-methyl GTP pull-down assay (Figure 6E). We also found an unexpected elevation of eIF4E expression in *Raptor*-deficient AML cells (Figure 6E), and binding of eIF4E to the cap structure appeared to be enhanced. These data suggest that increased production of eIF4E may overcome the inactivation of eIF4E by 4E-BP1.

Raptor-deficient AML stem cells show defective leukemia-initiating capacity. To evaluate the leukemia-initiating capacity of *Raptor*-deficient AML stem cells, we transplanted into recipient mice a limiting dilution series of K^+G^- AML cells isolated from *Raptor*$^{fl/fl}$*CreER* AML mice that had been injected (or not) with TAM. Transplantation of control AML cells promoted efficient development of leukemia with features identical to those of the original AML. Even when only 10 control AML cells were transplanted per mouse, 80% of recipients developed overt AML and died within 60 days (Figure 7A). In contrast, recipients injected with 10 or 100 *Raptor*-deficient AML cells did not die of overt leukemia. Although recipients injected with 1,000 *Raptor*$^{fl/fl}$ *CreER*$^{+TAM}$ AML cells developed leukemia, the emerging AML cells showed incomplete deletion of the *Raptor* gene. Thus, *Raptor* deficiency apparently has a negative impact on leukemia-initiating capacity.

To investigate the effect of *Raptor* deficiency on AML stem cell function, we first evaluated the colony-forming ability of various *Raptor*-deficient AML cell subpopulations in vitro. As expected, the undifferentiated AML cell population (K^+G^- cells) of control AML mice formed colonies at a much higher frequency than did differentiated AML cells (K^-G^+ cells) (Figure 7B). When *Raptor* was deleted by TAM administration, a dramatic reduction was observed in the number of colonies derived from K^+G^- AML cells.

To identify the reason for the failure of colony formation and leukemia propagation by *Raptor*-deficient AML stem cells, we analyzed the behavior of AML cells stimulated with several cytokines, because we assumed that both colony formation and the expansion of leu-

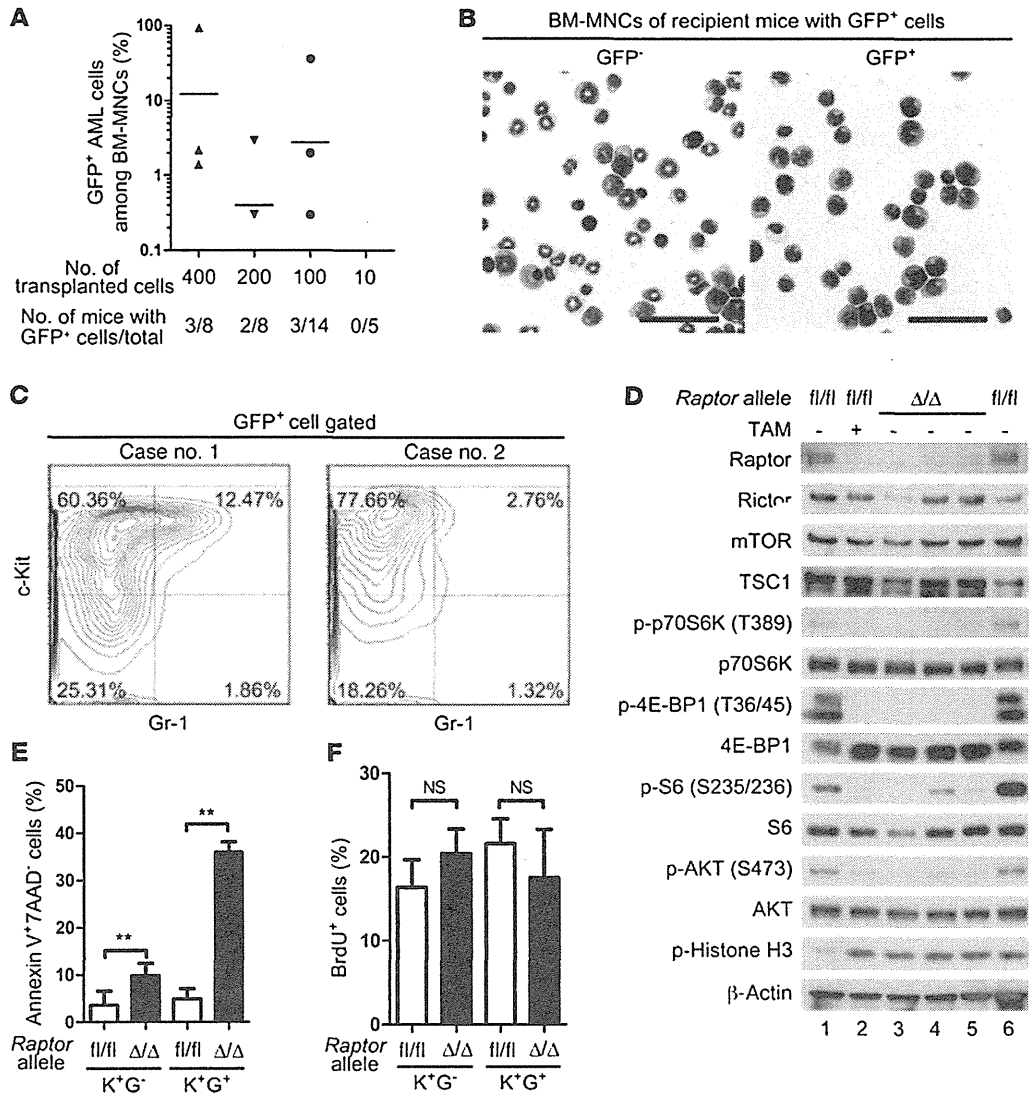

Figure 8

mTORC1-independent long-term survival of AML cells in vivo. (**A**) Presence of AML cells surviving long-term in BM. 10–400 K^+G^- cells from *Raptor*$^{fl/fl}$*CreER*$^{+TAM}$ AML mice were transplanted into recipients, and GFP expression was evaluated in BM-MNCs 100 days after transplantation. Data shown are the percentages of GFP^+ cells among total BM-MNCs. Horizontal lines are the mean percentages of GFP^+ cells in cases where GFP^+ cells were present. Numbers of mice possessing GFP^+ cells/total number of recipients are shown at the bottom of the panel. (**B**) Morphological analysis of *Raptor*$^{\Delta/\Delta}$ AML cells. GFP^- and GFP^+ cells were isolated from BM-MNCs of recipients possessing GFP^+ cells. Cells were stained with May-Grünwald/Giemsa. Scale bars: 50 μm. (**C**) Flow cytometric characterization of the AML cells in **A**. Results of two representative analyses are shown. (**D**) Phosphorylation of mTOR signaling pathway proteins in *Raptor*$^{\Delta/\Delta}$ (long-term *Raptor*-deficient) AML cells. Immunoblotting to detect the indicated proteins was performed on lysates of GFP^+ K^+G^- cells isolated from the following mice: lanes 1 and 6, *Raptor*$^{fl/fl}$*CreER*$^{-TAM}$ AML (fl/fl; TAM–, control); lane 2, *Raptor*$^{fl/fl}$*CreER*$^{+TAM}$ AML at 14 days post-TAM (fl/fl; TAM+); lanes 3–5, *Raptor*$^{\Delta/\Delta}$ AML (Δ/Δ). (**E** and **F**) Analysis of apoptosis and cell cycle in *Raptor*$^{\Delta/\Delta}$ AML cells. The apoptosis rate (**E**) and proportion of cells in the cell cycle (**F**) of the indicated subpopulations from *Raptor*$^{fl/fl}$*CreER*$^{-TAM}$ AML cells (fl/fl; TAM–, control) and *Raptor*$^{\Delta/\Delta}$ AML cells (Δ/Δ) were evaluated by using Annexin V/7AAD staining and BrdU incorporation, respectively. Data shown in **E** and **F** are the mean ± SD of Annexin V^+7AAD^- cells ($n = 4$) and $BrdU^+$ cells ($n = 4$), respectively. $^{**}P < 0.01$ (Student's *t* test).

kemia cells are supported by cytokine signals. We found that *Raptor*-deficient K^+G^- AML cells stimulated with the cytokines SCF, IL-3, and IL-6 showed an increase in apoptosis and a decrease in cell division (Figure 7, C and D). However, *Raptor* deficiency did not downregulate c-Kit (Figure 7E). These data indicate that failure of AML propagation when mTORC1 is inactivated is due to enhanced apoptosis and defective proliferation, but not accelerated differentiation.

Raptor-deficient AML stem cells can survive long-term in BM. To confirm that Raptor deficiency completely depletes AML cells after transplantation, we analyzed BM of the recipient mice injected with fewer than 1,000 *Raptor*$^{fl/fl}$*CreER*$^{+TAM}$ AML cells 100 days after transplantation. Surprisingly, we discovered that some recipient mice retained donor-derived leukemia cells (GFP^+) in their BM. Detailed examination revealed that these surviving GFP^+ cells were present

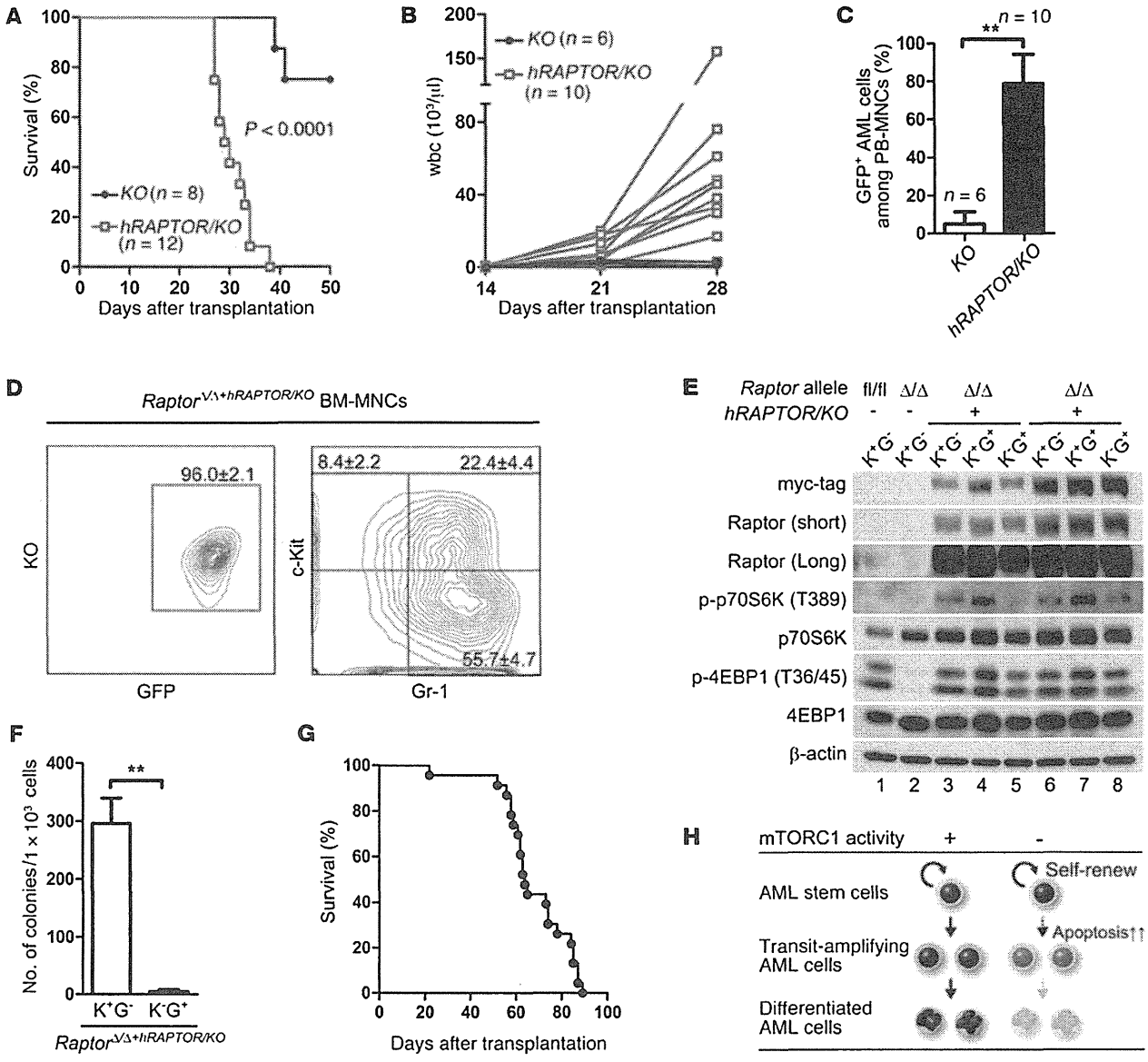

Figure 9

Restoration of leukemia-initiating capacity of long-term *Raptor*-deficient AML stem cells by mTORC1 reactivation. (**A**–**C**) Leukemia development upon restoration of Raptor. Recipient mice were transplanted with BM-MNCs (including $Raptor^{\Delta/\Delta}$ AML cells) infected with either control retrovirus expressing *KO* alone or retrovirus expressing *hRAPTOR* (*hRAPTOR/KO*). Survival (**A**), total number of wbc in PB (**B**), and the mean percentage ± SD of GFP⁺ cells in PB (**C**) of these recipients were analyzed 26–35 days after transplantation. For **A**, the *P* value was determined by the log-rank test. (**D**) Flow cytometric analysis of $Raptor^{\Delta/\Delta+hRAPTOR/KO}$ AML cells. Representative data for GFP/KO fluorescence (left) and c-Kit/Gr-1 expression (right) of BM-MNCs from the recipient mice in **A**–**C** are shown. Values are the mean percentage ± SD of the indicated subpopulations ($n = 7$). (**E**) Phosphorylation of mTOR signaling pathway proteins in $Raptor^{\Delta/\Delta+hRAPTOR/KO}$ AML cells. Immunoblotting to detect the indicated proteins was performed on lysates of the indicated AML cell subpopulations prepared from the following mice: lane 1, $Raptor^{fl/fl}CreER^{-TAM}$ (TAM-, control); lane 2, $Raptor^{\Delta/\Delta}$; lanes 3–5, $Raptor^{\Delta/\Delta+hRAPTOR/KO}$ (case 1); lanes 6–8, $Raptor^{\Delta/\Delta+hRAPTOR/KO}$ (case 2). (**F**) Colony-forming ability of $Raptor^{\Delta/\Delta+hRAPTOR/KO}$ AML cells. K⁺G⁻ or K⁻G⁺ (GFP⁺KO⁺) subpopulations isolated from among $Raptor^{\Delta/\Delta+hRAPTOR/KO}$ AML cells were cultured in semisolid medium for 7 days. Data are the mean colony number ± SD ($n = 3$). (**G**) The survival of recipient mice transplanted with 100 K⁺G⁻ $Raptor^{\Delta/\Delta+hRAPTOR/KO}$ AML cells was monitored ($n = 23$). (**H**) Model of the role of mTORC1 in AML stem cell regulation. See text for explanation. $^{**}P < 0.01$ (Student's *t* test).

in 8 of 30 recipients injected with 100–400 $Raptor^{fl/fl}CreER^{+TAM}$ AML cells (Figure 8A) and that the frequency of these leukemia cells in the BM of individuals was highly variable. The GFP⁺ cells were morphologically leukemic (Figure 8B). Interestingly, these animals showed no overt abnormalities of hematopoiesis in PB (Supplemental Figure 9, A and B). Recipient mice injected with only 10 $Raptor^{fl/fl}CreER^{+TAM}$ AML cells did not harbor any leukemia cells at 100 days after transplantation.

The AML cells that survived long-term in recipient BM exhibited AML stem cell phenotypes, as judged by the expression of cell surface markers (i.e., they were K^+G^-; Figure 8C). We confirmed that AML cells surviving long-term showed complete deletion of the *Raptor* gene and loss of the Raptor protein, and we refer to them as $Raptor^{\Delta/\Delta}$ AML cells (Figure 8D). $Raptor^{\Delta/\Delta}$ AML cells showed less phosphorylation of the mTORC1 target molecules p70S6K and 4E-BP1 (Figure 8D). Notably, extended survival of $Raptor^{\Delta/\Delta}$ AML cells was dependent on the in vivo microenvironment, as these cells did not form colonies in vitro (data not shown), just as we observed for the original AML cells prior to transplantation (Figure 7B). $Raptor^{\Delta/\Delta}$ AML cells showed increased apoptosis in vivo compared with control $Raptor^{fl/fl}CreER^{-TAM}$ AML cells, particularly in the K^+G^+ population (Figure 8E). The cell cycle status of $Raptor^{\Delta/\Delta}$ AML cells was comparable to that of controls (Figure 8F). These data suggest that AML stem cells lacking mTORC1 activity can survive long-term in the BM, but that the host animal survives because AML cells that propagate and differentiate are eliminated by apoptosis.

The self-renewal capacity of AML stem cells is sustained in the absence of mTORC1 activity. Finally, we asked whether the AML cells that survive long-term in the BM in the absence of mTORC1 activity are genuine AML stem cells. To this end, we devised a strategy to reintroduce Raptor into those $Raptor^{\Delta/\Delta}$ AML cells that survive long-term in vivo without mTORC1 activity. We prepared a retrovirus carrying the *hRAPTOR* gene labeled with Kusabira-Orange (*hRAPTOR/KO*) (Supplemental Figure 10, A–F) and used this vector, or a control retrovirus expressing *KO* alone, to infect total BM-MNCs from recipient mice harboring $Raptor^{\Delta/\Delta}$ AML cells. To avoid the death of $Raptor^{\Delta/\Delta}$ AML cells ex vivo, retroviral infection was performed with minimum incubation, followed by immediate transplantation into fresh recipients. Mice receiving $Raptor^{\Delta/\Delta}$ AML cells expressing the *hRAPTOR/KO* gene ($Raptor^{\Delta/\Delta+hRAPTOR/KO}$ AML cells) developed overt leukemia (Supplemental Figure 10G) and died rapidly (Figure 9A), whereas mice that received AML cells expressing the control *KO* gene did not. Levels of wbc expressing *hRAPTOR/KO* were greatly elevated in affected recipients by day 28 after transplantation (Figure 9, B and C). All GFP^+ AML cells also showed KO fluorescence (i.e., expressed the *hRAPTOR/KO* gene) (Figure 9D). Moreover, $Raptor^{\Delta/\Delta+hRAPTOR/KO}$ AML cells in BM exhibited a pattern of differentiation markers identical to that of control AML cells (Figure 9D), indicating that introduction of the *hRAPTOR* gene fully restored the original AML phenotype. Immunoblotting confirmed that the introduction of the *hRAPTOR/KO* gene had resulted in RAPTOR protein overexpression (Figure 9E). RAPTOR overexpression promoted increased levels of p-p70S6K and restored p–4E-BP1 levels to those seen in the original AML cells. The colony-forming ability of *Raptor*-deficient K^+G^- AML cells was also rescued by reintroduction of RAPTOR protein (Figure 9F). In addition, a sequential transplantation study showed that only 100 RAPTOR-expressing K^+G^- AML cells were required to efficiently generate overt AML in recipient mice, which resulted in their death within 89 days (Figure 9G). This indicates that the leukemia-initiating capacity was fully restored by reactivation of mTORC1. Together with our finding that $Raptor^{\Delta/\Delta}$ AML cells are cycling (Figure 8F), these data indicate that *Raptor*-deficient AML cells can self-renew and serve as AML stem cells.

Discussion

Distinct mechanisms control the tumor initiation and self-renewal properties of CSCs. It has been assumed that CSCs can survive and self-renew, contributing to cancer recurrence, even when a treatment is effective in reducing tumor mass. This is illustrated by the case of chronic myeloid leukemia patients treated with tyrosine kinase inhibitors (37, 38). These findings indicate that it is necessary to distinguish CSC self-renewal activity from tumor-initiating capacity. Here, we demonstrate that although mTORC1 inactivation eliminates AML cells that exhibit properties of transit-amplifying cells and differentiated cells, it does not affect the self-renewal activity of AML stem cells (Figure 9H). On the basis of these findings, we propose that tumor-initiating and -propagating properties should be considered separately from CSC self-renewal activity. Our observations could have substantial impact on investigations of mechanisms that allow residual CSCs to escape cancer treatment and drive tumor recurrence.

Essential role of mTORC1 in AML propagation. Appropriate regulation of survival and proliferation of transit-amplifying tumor cells is required for robust tumor initiation, which is associated with aggressiveness of tumors. In our study, most *Raptor*-deficient AML cells, particularly differentiated AML cells, showed a remarkable increase in apoptosis in vivo. In addition, *Raptor* deficiency led to a defect in proliferation in differentiated AML cells, but not undifferentiated cells. Thus, mTORC1 activity appears to play a critical role in proliferation and survival in vivo mainly in differentiated cells, rather than AML stem cells. Consistent with these in vivo observations, we found that *Raptor* deficiency enhanced apoptosis and reduced proliferation in AML cells stimulated by cytokine signals in vitro. Because AML cells propagate in vivo as transit-amplifying AML cells supported by cytokine signals, these findings suggest that mTORC1 inactivation results in defective AML propagation, leading to prolonged survival of AML mice.

The molecular mechanism of mTORC1-dependent AML propagation is unclear. Although previous studies reported that inhibition of 4E-BP phosphorylation is associated with the induction of apoptosis in tumors (39, 40), it was assumed that other molecules downstream of mTORC1 cooperatively contribute to AML propagation. To understand how mTORC1 supports AML propagation at the molecular level, we performed a quantitative phosphoproteomics study using the SILAC (stable isotope labeling with amino acids in cell culture) method and found numerous peptides that were dramatically de-phosphorylated by *Raptor* deficiency (T. Hoshii and N. Sugiyama, unpublished observations). Among these molecules, there were several known downstream targets of mTORC1, including Raptor, 4E-BP1/2, AKTS1 (also known as PRAS40), and LARP1 (26, 27). Decreased phosphorylation of AKTS1, as well as of 4E-BPs, is reportedly associated with apoptosis in tumor cells (41). Therefore, we assumed that mTORC1 inactivation affects the activities of these target molecules, which are regulated by their phosphorylation status, resulting in defective AML propagation.

Although rapamycin derivatives have been tested in AML patients in clinical trials, it has remained controversial whether such medications are effective (42–44). In our study, rapamycin treatment slightly prolonged the survival of AML mice, but it had a milder effect than *Raptor* deficiency. The difference is likely due to the limited effects of rapamycin on mTORC1 inhibition. We found that the inhibitory effects of rapamycin differed among mTORC1 targets. For example, rapamycin treatment effectively suppressed the phosphorylation of p70S6K but did not affect the phosphorylation of 4E-BP1, which is consistent with previous reports (24, 25). These data strongly suggest that a genetic approach is required to understand the bona fide effects of

mTORC1 inhibition in vivo. Thus, dissection of mTORC1 signaling pathways using the *Raptor*-deficient AML cells should provide critical evidence for identifying indicators or therapeutic targets to control the aggressiveness of leukemic diseases.

Self-renewal of AML stem cells lacking mTORC1. A particularly interesting and unexpected finding emerging from our work is that AML stem cells lacking mTORC1 activity can proliferate and survive long-term in vivo. Previous studies demonstrated that mTORC1 activity plays critical roles in cell proliferation in embryonic fibroblasts and cell lines (45, 46). The knockdown of *Raptor* or a decrease in serum concentration in culture inhibits cell proliferation. Because the proliferation is restored by 4E-BP1/2 deficiency, 4E-BPs are thought to be key regulators of cell proliferation when mTORC1 activity is downregulated (45). As expected, we found that embryonic fibroblasts lacking *Raptor* showed remarkable defects in cell proliferation (Supplemental Figure 1C). However, we unexpectedly observed that the cell cycle and self-renewing proliferation of AML stem cells in vivo were not altered by mTORC1 inactivation in our experiments. Because the phosphorylation of 4E-BP1 was dramatically suppressed in these cells, 4E-BP1–independent mechanisms of cell proliferation must support self-renewal of AML stem cells. Although 4E-BP1 phosphorylation reportedly induces cap-dependent protein translation, which controls the growth of individual cells, we found no evidence of an inhibitory effect of *Raptor* deficiency on the size or protein amount of AML stem cells. We confirmed that *Raptor* deficiency enhanced binding of 4E-BP1 to eIF4E due to 4E-BP1 hypophosphorylation. However, we unexpectedly found elevated eIF4E protein levels and enhanced eIF4E binding to cap structures in *Raptor*-deficient AML cells. Because eIF4E overexpression reportedly increases cell size and resistance to rapamycin treatment (41, 42), the increased presence of eIF4E protein on cap structures may compensate for the inhibition of eIF4E activity by 4E-BP1, leading to the retained cell growth and self-renewal in the absence of mTORC1.

Similar to what we observed in AML stem cells, we also found that *Raptor* deficiency did not cause defective phenotypes in GMP myeloid progenitor cells. Because AML stem cells likely originate from myeloid progenitors, the two types of cells may share the property of mTORC1 dependency (22). A possible compensatory mechanism for cell proliferation observed in *Raptor*-deficient GMP is mTORC1-independent regulation of the ribosomal protein S6 and eEF2K. Although S6 and eEF2K are substrates of p70S6K, it was also reported that p90 RSK can phosphorylate these proteins (28, 30). Activation of p90 RSK is dependent on Ras/ERK signaling. Study of hematopoietic progenitor cells with the K-ras^{G12D} mutation revealed that phosphorylation of S6 after GM-CSF stimulation is highly dependent on MEK/ERK signaling, but not on PI3K/AKT signaling (29). Therefore, such mTORC1-independent S6 and eEF2K phosphorylation may compensate for the lack of mTORC1 in supporting cell proliferation of GMPs. Unlike in GMPs, the phosphorylation of S6 was strongly inhibited in *Raptor*-deficient AML stem cells. However, the residual level of S6 activity supported by mTORC1-independent signaling may be enough to promote the self-renewal of AML stem cells.

It has been reported that mTORC1 inhibition activates autophagy, a protein degradation system, to generate energy for survival under conditions of stress or starvation (4). An interaction of Raptor and ULK1 mediates the incorporation of mTORC1 into the ULK1-Atg13-FIP200 complex, which is required for autophagy, and mTOR phosphorylates ULK1 and Atg13, indicating that autophagy is directly regulated by mTORC1 (47). Therefore, autophagy induced by *Raptor* deficiency may support the survival of AML stem cells in vivo. In our preliminary experiments, we did not observe an increase in LC3-II in *Raptor*-deficient AML stem cells (our unpublished observations). Thus, the roles of autophagy in AML stem cell survival are unclear in our experiments. We believe that it is necessary to investigate how autophagy is involved in the survival of AML stem cells, because such information may be important for developing a strategy to use a combination of mTORC1 and autophagy inhibitors to eradicate AML stem cells.

A recent study revealed that AKT is a key regulator for the maintenance of AML stem cells (48). Suppression of AKT activity is reported to be essential for inhibiting the differentiation of leukemia stem cells and supporting their self-renewal ability in MLL-AF9–driven AML. Feedback activation of the PI3K/AKT pathway is triggered by inhibition of Grb10 and/or activation of IRS after acute mTORC1 inactivation (26, 27). On the other hand, prolonged rapamycin treatment is reported to suppress AKT via the disassembly of the mTORC2 complex in certain cell types (49). In our study, we observed that AKT phosphorylation was attenuated in *Raptor*$^{\Delta/\Delta}$ AML cells. We found that *Raptor* deficiency did not affect the expression level of Rictor, an essential component of mTORC2, but it is possible that long-term inactivation of mTORC1 in *Raptor*-deficient AML cells affects the assembly and activity of mTORC2, leading to inhibition of AKT, in the same manner as prolonged rapamycin treatment (49). To investigate whether mTORC2 is involved in regulating AKT for the survival of AML stem cells, a genetic study using *mTOR* or *Rictor* mutant mice would be necessary. Thus, although the mechanism is unclear, the suppression of AKT in *Raptor*$^{\Delta/\Delta}$ AML stem cells may suppress the differentiation of AML stem cells and support their self-renewal activity.

Our results also suggest that mTORC1 inactivation might prevent the differentiation of AML stem cells in a cell-intrinsic manner, because we found that *Raptor*-deficient AML cells had higher c-Kit expression than controls in culture (Figure 7E). Unknown microenvironmental factors may enhance this effect of mTORC1, because we observed a remarkable increase in the absolute number of AML stem cells in vivo (Figure 5E). These findings lead to the intriguing idea that mTORC1 inhibition enhances self-renewal activity in combination with microenvironmental factors. Further dissection of the regulation of *Raptor*-deficient AML stem cells is required to identify the critical factors or functions of AML stem cells. Increased understanding of the mechanisms by which AML stem cells self-renew should suggest novel therapeutic approaches that will successfully eradicate CSCs.

Methods

Mice. To generate mice bearing an inducible conditional deletion of *Raptor*, we obtained BAC clones (BACPAC Resources Center) that encode the mouse genomic DNA sequences encompassing the region containing exon 2 of the *Raptor* gene. Genomic DNA fragments were inserted into a plasmid containing paired loxP sites and FRT recombination sites flanking a neomycin selection cassette. A diphtheria toxin cassette was added downstream of the 3′ arm to reduce the frequency of random insertion. This vector was transfected into feeder-free TT2 ES cells (derived from the TT2 ES cell line; ref. 50) by electroporation, and the cells were subjected to G418 selection as previously described (51). ES clones possessing the recombined allele were identified by PCR and Southern blot analyses. ES cells were aggregated with ICR morulae, and chimeras were obtained. The chimeric mice were crossed with *CAG-Flp* mice (51) to remove the neo cassette and generate mice with

the *Raptor*^{fl} allele. Mice with the *Raptor*^{fl} allele were crossed with *Rosa26-CreER*^{T2} mice (52) obtained from Tyler Jacks (Massachusetts Institute of Technology, Cambridge, Massachusetts, USA), and the resulting progeny were backcrossed for at least 6 generations onto the C57BL/6-CD45.2 genetic background. All mice used as transplantation recipients in this study were 8- to 12-week-old C57BL/6-CD45.1 mice (Sankyo Lab).

PCR primers. The primers used to identify the *Raptor* WT, floxed, and deleted alleles in PCR analyses were raptor-a (AAAGACAAACCAGTGAGCAAGGGG), raptor-b (GGAGCTTCCTTATCGTGAATCTCC), and raptor-c (CTGGGAACTGCGATAAGCCG).

Blood collection and analysis. Total BM cells were obtained from femoral and tibial bones by aspiration. MNCs were isolated from total BM cells by density gradient centrifugation using Lymphoprep (Axis-Shield). PB cells were collected from the postorbital vein and suspended in diluted heparin solution. Blood counts were performed using Celltac (NIHON KOHDEN). MNCs in PB were isolated by dextran sedimentation and ammonium chloride lysis of erythrocytes using standard procedures.

Tamoxifen and rapamycin treatments. To analyze the effect of *Raptor* deficiency in mice without transplantation, we treated 8-week-old mice with TAM (Sigma-Aldrich). TAM was dissolved in corn oil (Sigma-Aldrich) to 20 mg/ml and injected i.p. at 150 mg/kg/d for 5 consecutive days. The corn oil diluent was injected as the control. For TAM treatment of cells in vitro, 1 μM 4-hydroxytamoxifen (4-OHT; Sigma-Aldrich) was added to the culture medium. Rapamycin (Sirolimus, LC Laboratories) was dissolved in ethanol to 10 mg/ml stock solution. For in vivo experiments, the rapamycin stock solution was diluted to make a final concentration of 0.4 mg/ml rapamycin in 5% PEG-400, 5% Tween 80, and 4% ethanol. Rapamycin (4 mg/kg) or vehicle (5% PEG-400, 5% Tween 80, and 4% ethanol) was injected i.p. every other day. For rapamycin treatment of cells in vitro, 100 nM rapamycin (Cell Signaling Technology) dissolved in methanol was added to the culture medium.

Flow cytometry. mAbs recognizing the following markers were used for flow cytometry: Sca-1 (E13-161.7), CD4 (L3T3), CD8 (clone 53-6.7), B220 (RA3-6B2), TER119 (Ly-76), Gr-1 (RB6-8C5), Mac-1 (M1/70), IL-7Rα chain (B12-1), FcγIII/II receptor (2.4G2), CD34 (RAM34), IgM (II/41), CD45.1 (A20), CD45.2 (clone 104), and c-Kit (2B8) (all from BD Biosciences or eBiosciences). Marker analyses were performed using a FACSCanto II (BD Biosciences), and cell sorting was performed using a FACSAria (BD Biosciences).

For analysis of intracellular phosphorylated proteins, 5×10^4 cells were fixed in 4% paraformaldehyde at 37°C for 10 minutes and permeabilized in 90% cold methanol for at least 30 minutes. Cells were then washed with staining buffer (5% FBS in PBS) and incubated at room temperature for 1 hour with Alexa Fluor 647–conjugated anti–p-S6 (S235/236) plus Alexa Fluor 488–conjugated anti–p-4E-BP1 (T37/46; T36/T45 for *Mus musculus*) Abs, or Alexa Fluor 647–conjugated rabbit mAb IgG isotype control and Alexa Fluor 488–conjugated rabbit mAb IgG isotype control. Immunostained cells were washed with staining buffer and analyzed by flow cytometry.

Colony-forming assay. $K^+S^+L^-$ cells and GMPs isolated from BM of non-AML mice, or $GFP^+K^+G^-$ or K^-G^+ cells isolated from BM of AML mice, were cultured for 10 or 7 days, respectively, in semisolid medium containing 50 ng/ml recombinant murine stem cell factor (rmSCF), 10 ng/ml rmIL-3, 10 ng/ml rmIL-6, and 3 U/ml recombinant human erythropoietin (rhEPO) (Methocult GF M3434, Stem Cell Technologies) at 37°C in humidified air containing 5% CO_2. Colonies containing more than 40 cells were counted under a microscope.

Cell cycle. To analyze the cell cycle of hematopoietic cells in vivo, BrdU (100 mg/kg; Sigma-Aldrich) was injected i.p. into mice. After 2 hours, cells were collected, immunostained to detect surface markers, and purified using a cell sorter. For analysis of the cell cycle of AML cells in vitro, cells were cultured with medium supplemented with 10 μM BrdU for 30 minutes. Cells were fixed in 70% ethanol at –30°C for 16 hours. The DNA in fixed cells was denatured by treatment with 2 N HCl at room temperature for 30 minutes, followed by neutralization using 0.05 M borax buffer. Incorporated BrdU was labeled by incubation with FITC-conjugated anti-BrdU Ab (BD Biosciences) at room temperature for 1 hour. Labeled cells were resuspended in PBS containing 1% bovine serum albumin and 7-aminoactinomycin D (7AAD; BD Biosciences) plus RNase A (Sigma-Aldrich), and BrdU-positive cells were quantified by flow cytometry.

Apoptosis. For TUNEL assays of floating cells, cells were fixed in 4% paraformaldehyde and permeabilized in 70% ethanol at –30°C for 16 hours. For TUNEL assays of small intestine, small intestines were fixed with 4% paraformaldehyde, and paraffin-embedded tissues were sectioned, dewaxed, and rehydrated. Fragmented DNA was labeled with fluorescein-12-dUTP using the DeadEnd Fluorometric TUNEL System (Promega) and analyzed by flow cytometry or FV1000 confocal microscopy (Olympus). For Annexin V staining, cells were incubated with PE-conjugated Annexin-V and 7AAD in Annexin V binding buffer (BD Biosciences) in accordance with the manufacturer's protocol.

Competitive repopulation assay in vivo. Tester BM-MNCs (1×10^6) from *Raptor*$^{fl/fl}$ or *Raptor*$^{fl/fl}$*CreER* mice (CD45.2) and competitor WT BM-MNCs (1×10^6, CD45.1/2) were transplanted into lethally irradiated (9.5 Gy) recipient mice ($CD45.1^+$). At 8 weeks after transplantation, TAM was administered to the recipients as described above. Hematopoietic cells regenerated from tester cells or competitor cells were examined by flow cytometry.

Gene transduction by retroviral infection. The pMSCV-*MLL-AF9*-ires-*eGFP* vector was a gift from Akihiko Yokoyama, Kyoto University, Kyoto, Japan. The Myc-tagged human *RAPTOR* gene was a gift from David M. Sabatini, Whitehead Institute, Cambridge, Massachusetts, USA (Addgene plasmid 1859) and was cloned into the pGCDNsam-ires-*eGFP* or pGCDNsam-ires-*hKO* vector (both gifts from Masafumi Onodera, National Center for Child Health and Development, Tokyo, Japan). Retroviral packaging cells (Plat-E, ref. 53; gift from Toshio Kitamura, University of Tokyo, Tokyo, Japan) were transiently transfected with the above plasmids using calcium phosphate, and culture supernatants containing retroviruses were collected 48 hours after transfection.

For retroviral gene transduction, three cell type–specific protocols were used: (a) $K^+S^+L^-$ cells isolated from *Raptor*$^{fl/fl}$ or *Raptor*$^{fl/fl}$*CreER* mice were cultured overnight in serum-free S-Clone SF-03 medium (Sanko Junyaku) supplemented with 100 ng/ml recombinant human thrombopoietin (PeproTech) plus 100 ng/ml rmSCF (Wako Pure Chemical). Cells were then infected with retroviruses carrying *MLL-AF9*-ires-*eGFP* or *hRAPTOR*-ires-*eGFP* using CombiMag (OZ Biosciences) in accordance with the manufacturer's instructions. (b) AML cells were cultured for several days in RPMI 1640 medium supplemented with 10% FBS and 10 ng/ml rmIL-3 (Wako Pure Chemical). Cells were infected with a retroviral vector carrying *hRAPTOR*-ires-*hKO* using 8 μg/ml Polybrene. Two days after infection, KO^+ cells were collected using a cell sorter and subjected to colony-forming assays as described above. (c) For *Raptor*$^{\Delta/\Delta}$ AML cells, freshly isolated BM cells from recipient mice possessing *Raptor*$^{\Delta/\Delta}$ AML cells were suspended in RPMI 1640 medium supplemented with 20 ng/ml rmSCF, 10 ng/ml rmIL-3, 10 ng/ml rmIL-6, and 10 ng/ml rmIL-7 and containing 8 μg/ml Polybrene. Spin infection was performed by adding retrovirus carrying *hRAPTOR*-ires-*KO* or *KO* to the suspended cells and centrifuging at 1,500 *g* for 1 hour. After a first round of spin infection, cells underwent a second round of spin infection using fresh retrovirus. Then, 2×10^6 infected cells were cultured for an additional 2 hours before transplantation into lethally irradiated (9.5 Gy) syngeneic recipient mice.

Murine AML model. $K^+S^+L^-$ cells isolated from *Raptor*$^{fl/fl}$, *Raptor*$^{+/+}$*CreER*, or *Raptor*$^{fl/fl}$*CreER* mice were infected with retrovirus carrying *MLL-AF9*-ires-*eGFP* as described above and transplanted into lethally irradiated syngeneic mice along with 2×10^5 normal BM-MNCs (rescue cells). AML-

like disease developed in these AML mice between 34 and 124 days after transplantation (mean, 76.7 days; SD, 27.8). After the appearance of AML symptoms, 5×10^5 BM-MNCs from the AML mice were transplanted intravenously into lethally irradiated syngeneic recipients along with 5×10^5 normal BM-MNCs. Administration of TAM (150 mg/kg/d for 5 days, i.p.) was begun 3 days after transplantation. Corn oil was injected as the diluent control in the same manner. For the limiting dilution transplantation assay to evaluate leukemia-initiating capacity, $GFP^+c\text{-}Kit^+Gr\text{-}1^-$ AML cells were collected from recipient mice 14 days after the last TAM injection and transplanted into lethally irradiated syngeneic recipients along with 2×10^5 normal BM-MNCs.

Immunoblotting. Cells (5×10^4) of various subpopulations were purified by cell sorting and lysed in SDS sample buffer containing proteinase inhibitor (P8340, Sigma-Aldrich), phosphatase inhibitor cocktail 2 (P5726, Sigma-Aldrich), and phosphatase inhibitor cocktail 3 (P0044, Sigma-Aldrich). Lysis was completed via ultrasonication, and proteins were denatured by boiling. Denatured proteins were separated on a 5%–20% acrylamide gradient gel and transferred to a PVDF membrane (GE Healthcare). Blots were incubated with Abs against Raptor, mTOR, Rictor, TSC1, p-4E-BP1 (T37/46; T36/T45 for *M. musculus*), p-4E-BP1 (S65; S64 for *M. musculus*), p-4E-BP1 (T70; T69 for *M. musculus*), 4E-BP1, p-S6 (S235/236), p-S6 (S240/244), S6, p-p70S6K (T389), p70S6K, p-AKT (T308), p-AKT (S473), and eIF4E (all from Cell Signaling Technologies), p-histone H3 (Upstate), β-actin (Sigma-Aldrich), and Myc tag (MBL). Immunocomplexes were labeled using an HRP-conjugated anti-mouse Ab (GE Healthcare) or anti-rabbit Ab (Cell Signaling Technology) and visualized using Immunostar LD (Wako) with ImageQuant LAS 4000 (GE Healthcare).

Histochemical staining. For May-Grünwald/Giemsa staining, cells purified by cell sorting were centrifuged onto glass slides and stained with May-Grünwald solution (MUTO Pure Chemicals) for 3 minutes. Subsequently, the slides were washed with distilled water for 3 minutes and stained with Giemsa solution (MUTO Pure Chemicals) for 10 minutes. For hematoxylin & eosin staining, rehydrated paraffin-embedded tissue sections were stained with Mayer's hematoxylin solution (Wako) for 5 minutes and washed with water for 5 minutes. The slides were then stained with eosin solution (Wako) for 10 seconds. Cells and tissues were visualized with Axio Imager A1 microscopes (Zeiss).

Protein quantification. For the colorimetric detection and quantification of total protein, cells (5×10^5) were purified by cell sorting and lysed in Cell Lysis Buffer (Cell Signaling Technology) containing proteinase inhibitor (P8340, Sigma-Aldrich). Lysis was completed via ultrasonication and quantified with bicinchoninic acid (BCA) protein assay reagent (Pierce). For silver staining of protein, cells (5×10^4) were lysed in SDS sample buffer containing proteinase inhibitor and phosphatase inhibitor cocktail. Denatured proteins were separated in a 5%–20% acrylamide gradient gel and then stained with a Silver Stain II Kit *Wako* (Wako).

7-methyl GTP pull-down assay. Cells (1×10^6) from each population were collected by cell sorter and lysed with lysis buffer (50 mM Tris pH 7.5, 150 mM KCl, 5 mM 2-ME, 1 mM EDTA, proteinase inhibitor, phosphatase inhibitor). The samples were completely lysed via ultrasonication and incubated with 7-methyl GTP-Sepharose 4B beads (GE Healthcare) at 4°C. After 16 hours of incubation, the beads were washed twice with lysis buffer. The beads were suspended in SDS sample buffer and denatured by boiling. Precipitated proteins were detected by Western blot analysis, and the 4E-BP1/eIF4E ratio was measured using ImageJ software (http://rsbweb.nih.gov/ij/).

Statistics. Statistical differences were determined using the unpaired Student's *t*-test (2-tailed) for *P*-values, and the log-rank (Mantel-Cox) test for survival curves.

Study approval. Animal care was in accordance with the guidelines for animal and recombinant DNA experiments of Kanazawa University or Kumamoto University. Animal studies were approved by the Committee on Animal Experimentation of Kanazawa University and the Ethics Committee of the Center for Animal Resources and Development, Kumamoto University.

Acknowledgments

We thank Tyler Jacks for providing *Rosa26-CreER^{T2}* mice; Akihiko Yokoyama for the pMSCV-*MLL-AF9*-ires-*eGFP* vector; Masafumi Onodera for the pGCDNsam-ires-*eGFP* and pGCDNsam-ires-*hKO* vectors; Toshio Kitamura for Plat-E retroviral packaging cells; Minoru Terashima for technical advice; and Miyako Takegami, Kazue Sawa, and Yumi Sakumura for expert technical support. We also thank members of the Hirao laboratory for helpful discussions. T. Hoshii was supported by a Grant-in-Aid for Young Scientists (B) and a Grant-in-Aid for Scientific Research on Innovative Areas "Cell Fate" from the Ministry of Education, Culture, Sports, Science and Technology, Japan. A. Hirao was supported by a Grant-in-Aid for Scientific Research on Innovative Areas and the Project for Development of Innovative Research on Cancer Therapeutics (P-DIRECT) from the Ministry of Education, Culture, Sports, Science and Technology, Japan, and by a grant from the Japan Science and Technology Agency (JST), Core Research for Evolution Science and Technology (CREST).

Received for publication December 5, 2011, and accepted in revised form April 4, 2012.

Address correspondence to: Atsushi Hirao, Division of Molecular Genetics, Cancer and Stem Cell Research Program, Cancer Research Institute, Kanazawa University, Kakuma-machi, Kanazawa, Ishikawa 920-1192, Japan. Phone: 81762646755; Fax: 81762344508; E-mail: ahirao@staff.kanazawa-u.ac.jp.

1. Ma XM, Blenis J. Molecular mechanisms of mTOR-mediated translational control. *Nat Rev Mol Cell Biol.* 2009;10(5):307–318.
2. Ramanathan A, Schreiber SL. Direct control of mitochondrial function by mTOR. *Proc Natl Acad Sci U S A.* 2009;106(52):22229–22232.
3. Cunningham JT, Rodgers JT, Arlow DH, Vazquez F, Mootha VK, Puigserver P. mTOR controls mitochondrial oxidative function through a YY1-PGC-1alpha transcriptional complex. *Nature.* 2007;450(7170):736–740.
4. Rabinowitz JD, White E. Autophagy and metabolism. *Science.* 2010;330(6009):1344–1348.
5. Alessi DR, Pearce LR, Garcia-Martinez JM. New insights into mTOR signaling: mTORC2 and beyond. *Sci Signal.* 2009;2(67):pe27.
6. Guertin DA, et al. Ablation in mice of the mTORC components raptor, rictor, or mLST8 reveals that mTORC2 is required for signaling to Akt-FOXO and PKCalpha, but not S6K1. *Dev Cell.* 2006;11(6):859–871.
7. Jacinto E, et al. SIN1/MIP1 maintains rictor-mTOR complex integrity and regulates Akt phosphorylation and substrate specificity. *Cell.* 2006;127(1):125–137.
8. Polak P, Cybulski N, Feige JN, Auwerx J, Ruegg MA, Hall MN. Adipose-specific knockout of raptor results in lean mice with enhanced mitochondrial respiration. *Cell Metab.* 2008;8(5):399–410.
9. Bentzinger CF, et al. Skeletal muscle-specific ablation of raptor, but not of rictor, causes metabolic changes and results in muscle dystrophy. *Cell Metab.* 2008;8(5):411–424.
10. Chen C, Liu Y, Liu R, Ikenoue T, Guan KL, Zheng P. TSC-mTOR maintains quiescence and function of hematopoietic stem cells by repressing mitochondrial biogenesis and reactive oxygen species. *J Exp Med.* 2008;205(10):2397–2408.
11. Gan B, et al. mTORC1-dependent and -independent regulation of stem cell renewal, differentiation, and mobilization. *Proc Natl Acad Sci U S A.* 2008;105(49):19384–19389.
12. Lee JY, et al. mTOR activation induces tumor suppressors that inhibit leukemogenesis and deplete hematopoietic stem cells after Pten deletion. *Cell Stem Cell.* 2010;7(5):593–605.
13. Nardella C, et al. Aberrant Rheb-mediated mTORC1 activation and Pten haploinsufficiency are cooperative oncogenic events. *Genes Dev.* 2008;22(16):2172–2177.
14. Yilmaz OH, et al. Pten dependence distinguishes

haematopoietic stem cells from leukaemia-initiating cells. *Nature*. 2006;441(7092):475–482.
15. Zhang J, et al. PTEN maintains haematopoietic stem cells and acts in lineage choice and leukaemia prevention. *Nature*. 2006;441(7092):518–522.
16. Reya T, Morrison SJ, Clarke MF, Weissman IL. Stem cells, cancer, and cancer stem cells. *Nature*. 2001;414(6859):105–111.
17. Somervaille TC, Cleary ML. Identification and characterization of leukemia stem cells in murine MLL-AF9 acute myeloid leukemia. *Cancer Cell*. 2006;10(4):257–268.
18. Krivtsov AV, et al. Transformation from committed progenitor to leukaemia stem cell initiated by MLL-AF9. *Nature*. 2006;442(7104):818–822.
19. Huntly BJ, et al. MOZ-TIF2, but not BCR-ABL, confers properties of leukemic stem cells to committed murine hematopoietic progenitors. *Cancer Cell*. 2004;6(6):587–596.
20. Cozzio A, Passegue E, Ayton PM, Karsunky H, Cleary ML, Weissman IL. Similar MLL-associated leukemias arising from self-renewing stem cells and short-lived myeloid progenitors. *Genes Dev*. 2003;17(24):3029–3035.
21. Lavau C, Luo RT, Du C, Thirman MJ. Retrovirus-mediated gene transfer of MLL-ELL transforms primary myeloid progenitors and causes acute myeloid leukemias in mice. *Proc Natl Acad Sci U S A*. 2000;97(20):10984–10989.
22. Goardon N, et al. Coexistence of LMPP-like and GMP-like leukemia stem cells in acute myeloid leukemia. *Cancer Cell*. 2011;19(1):138–152.
23. Somervaille TC, et al. Hierarchical maintenance of MLL myeloid leukemia stem cells employs a transcriptional program shared with embryonic rather than adult stem cells. *Cell Stem Cell*. 2009; 4(2):129–140.
24. Wang X, Beugnet A, Murakami M, Yamanaka S, Proud CG. Distinct signaling events downstream of mTOR cooperate to mediate the effects of amino acids and insulin on initiation factor 4E-binding proteins. *Mol Cell Biol*. 2005;25(7):2558–2572.
25. Choo AY, Yoon SO, Kim SG, Roux PP, Blenis J. Rapamycin differentially inhibits S6Ks and 4E-BP1 to mediate cell-type-specific repression of mRNA translation. *Proc Natl Acad Sci U S A*. 2008;105(45):17414–17419.
26. Hsu PP, et al. The mTOR-regulated phosphoproteome reveals a mechanism of mTORC1-mediated inhibition of growth factor signaling. *Science*. 2011;332(6035):1317–1322.
27. Yu Y, et al. Phosphoproteomic analysis identifies Grb10 as an mTORC1 substrate that negatively regulates insulin signaling. *Science*. 2011; 332(6035):1322–1326.
28. Roux PP, et al. RAS/ERK signaling promotes site-specific ribosomal protein S6 phosphorylation via RSK and stimulates cap-dependent translation. *J Biol Chem*. 2007;282(19):14056–14064.
29. Van Meter ME, et al. K-RasG12D expression induces hyperproliferation and aberrant signaling in primary hematopoietic stem/progenitor cells. *Blood*. 2007;109(9):3945–3952.
30. Wang X, Li W, Williams M, Terada N, Alessi DR, Proud CG. Regulation of elongation factor 2 kinase by p90(RSK1) and p70 S6 kinase. *EMBO J*. 2001;20(16):4370–4379.
31. Wang Y, et al. The Wnt/beta-catenin pathway is required for the development of leukemia stem cells in AML. *Science*. 2010;327(5973):1650–1653.
32. O'Reilly KE, et al. mTOR inhibition induces upstream receptor tyrosine kinase signaling and activates Akt. *Cancer Res*. 2006;66(3):1500–1508.
33. Sun SY, et al. Activation of Akt and eIF4E survival pathways by rapamycin-mediated mammalian target of rapamycin inhibition. *Cancer Res*. 2005;65(16):7052–7058.
34. Kim DH, et al. mTOR interacts with raptor to form a nutrient-sensitive complex that signals to the cell growth machinery. *Cell*. 2002;110(2):163–175.
35. Brunn GJ, et al. Phosphorylation of the translational repressor PHAS-I by the mammalian target of rapamycin. *Science*. 1997;277(5322):99–101.
36. Beretta L, Gingras AC, Svitkin YV, Hall MN, Sonenberg N. Rapamycin blocks the phosphorylation of 4E-BP1 and inhibits cap-dependent initiation of translation. *EMBO J*. 1996;15(3):658–664.
37. Michor F, et al. Dynamics of chronic myeloid leukaemia. *Nature*. 2005;435(7046):1267–1270.
38. Roeder I, Horn M, Glauche I, Hochhaus A, Mueller MC, Loeffler M. Dynamic modeling of imatinib-treated chronic myeloid leukemia: functional insights and clinical implications. *Nat Med*. 2006;12(10):1181–1184.
39. Nishioka C, Ikezoe T, Yang J, Yokoyama A. Inhibition of MEK/ERK signaling induces apoptosis of acute myelogenous leukemia cells via inhibition of eukaryotic initiation factor 4E-binding protein 1 and down-regulation of Mcl-1. *Apoptosis*. 2010;15(7):795–804.
40. She QB, et al. 4E-BP1 is a key effector of the oncogenic activation of the AKT and ERK signaling pathways that integrates their function in tumors. *Cancer Cell*. 2010;18(1):39–51.
41. Madhunapantula SV, Sharma A, Robertson GP. PRAS40 deregulates apoptosis in malignant melanoma. *Cancer Res*. 2007;67(8):3626–3636.
42. Recher C, et al. Antileukemic activity of rapamycin in acute myeloid leukemia. *Blood*. 2005; 105(6):2527–2534.
43. Rizzieri DA, et al. A phase 2 clinical trial of deforolimus (AP23573, MK-8669), a novel mammalian target of rapamycin inhibitor, in patients with relapsed or refractory hematologic malignancies. *Clin Cancer Res*. 2008;14(9):2756–2762.
44. Yee KW, et al. Phase I/II study of the mammalian target of rapamycin inhibitor everolimus (RAD001) in patients with relapsed or refractory hematologic malignancies. *Clin Cancer Res*. 2006;12(17):5165–5173.
45. Dowling RJ, et al. mTORC1-mediated cell proliferation, but not cell growth, controlled by the 4E-BPs. *Science*. 2010;328(5982):1172–1176.
46. Fingar DC, Richardson CJ, Tee AR, Cheatham L, Tsou C, Blenis J. mTOR controls cell cycle progression through its cell growth effectors S6K1 and 4E-BP1/eukaryotic translation initiation factor 4E. *Mol Cell Biol*. 2004;24(1):200–216.
47. Hosokawa N, et al. Nutrient-dependent mTORC1 association with the ULK1-Atg13-FIP200 complex required for autophagy. *Mol Biol Cell*. 2009;20(7):1981–1991.
48. Sykes SM, et al. AKT/FOXO signaling enforces reversible differentiation blockade in myeloid leukemias. *Cell*. 2011;146(5):697–708.
49. Sarbassov DD, et al. Prolonged rapamycin treatment inhibits mTORC2 assembly and Akt/PKB. *Mol Cell*. 2006;22(2):159–168.
50. Yagi T, et al. A novel ES cell line, TT2, with high germline-differentiating potency. *Anal Biochem*. 1993;214(1):70–76.
51. Taniwaki T, et al. Characterization of an exchangeable gene trap using pU-17 carrying a stop codon-beta geo cassette. *Dev Growth Differ*. 2005;47(3):163–172.
52. Ventura A, et al. Restoration of p53 function leads to tumour regression in vivo. *Nature*. 2007; 445(7128):661–665.
53. Morita S, Kojima T, Kitamura T. Plat-E: an efficient and stable system for transient packaging of retroviruses. *Gene Ther*. 2000;7(12):1063–1066.

genesis 50:758–765 (2012)

TECHNOLOGY REPORT

A Cre Knock-In Mouse Line on the *Sickle Tail* Locus Induces Recombination in the Notochord and Intervertebral Disks

Koichiro Abe,[1] Kimi Araki,[2] Maya Tanigawa,[1] Kei Semba,[2] Takashi Ando,[2] Masahiro Sato,[3] Daisuke Sakai,[4] Akihiko Hiyama,[4] Joji Mochida,[4] and Ken-Ichi Yamamura[2]*

[1]Division of Basic Medical Science and Molecular Medicine, Tokai University School of Medicine, Kanagawa, Japan

[2]Institute of Resource Development and Analysis, Center for Animal Resources and Development, Kumamoto University, Kumamoto, Japan

[3]Section of Gene Expression Regulation, Frontier Science Research Center, Kagoshima University, Kagoshima, Japan

[4]Department of Orthopedic Surgery, Tokai University School of Medicine, Kanagawa, Japan

Received 2 March 2012; Revised 11 April 2012; Accepted 14 April 2012

Summary: *Sickle tail* (*Skt*) was originally identified by gene trap mutagenesis in mice, and the trapped gene is highly expressed in the notochord, intervertebral discs (IVD), and mesonephros. Here, we report the generation of Skt^{cre} mice expressing Cre recombinase in the IVD due to target insertion of the *cre* gene into the *Skt* locus by recombinase-mediated cassette exchange. Crossing a conditional lacZ Reporter (R26R), Cre expression from the Skt^{cre} allele specifically activates β-galactosidase expression in the whole notochord from E9.5 onwards. In E15.5 Skt^{cre};R26R embryos, reporter activity was detected in the nucleus pulposus and in a portion of the annulus fibrosus, resulting in expansion of Cre-expressing cells in the adult IVD. Reporter activity was also seen in the Skt^{cre};R26R mesonephros at E15.5. These results suggest that Skt^{cre} mice are useful for exploring the fate specification of notochordal cells and creating models for IVD-related skeletal diseases. genesis 50:758–765 , 2012. © 2012 Wiley Periodicals, Inc.

Key words: Skt^{cre}; disc-specific conditional knockout in the spine

INTRODUCTION

Intervertebral discs (IVD) are partially movable joints that connect adjacent vertebral bodies, providing flexibility and integrity to the spine. IVD degeneration is, therefore, strongly implicated as a cause of low back pain and impaired mobility (Freemont, 2009; Smith *et al.*, 2011). Although research on cell-based therapies is emerging for the damaged or traumatized IVD (Sakai, 2008), most of the popular surgical procedures do not preserve function of the IVD. The IVD is composed of two different functional tissues, the "inner" nucleus pulposus (NP) and the "outer" annulus fibrosus (AF). In general, the AF facilitates joint mobility and stability, and the NP distributes compressive forces between vertebral bodies. Developmentally, the NP and AF are derived from the notochord and somite, respectively (Risbud *et al.*, 2010; Smith *et al.*, 2011; Walmsley, 1953). Although the molecular mechanisms of notochord and somite development in early embryogenesis have been well characterized (Christ *et al.*, 2004; Saga and Takeda, 2001; Stemple, 2005), those of IVD formation in organogenesis are not fully understood.

The Cre/*lox*P system has emerged as a powerful tool for both conditional gene targeting and cell lineage analysis (Nagy, 2000). For Cre-mediated recombination in the IVD, the *P0*-Cre transgenic line (Yamauchi *et al.*, 1999) and the *Shhcre* knock-in line (*Shh* for *Sonic hedgehog*)(Choi *et al.*, 2008) are available. *P0* and *Shh*

*Correspondence to: K.-I. Yamamura, Institute of Resource Development and Analysis, Center for Animal Resources and Development, Kumamoto University, Kumamoto, Japan.
E-mail: yamamura@gpo.kumamoto-u.ac.jp

Contract grant sponsor: Tokai University School of Medicine Research Aid; Contract grant sponsor: Japan Society for Promotion of Science (JSPS), Contract grant number: 22930024.
Published online 22 April 2012 in
Wiley Online Library (wileyonlinelibrary.com).
DOI: 10.1002/dvg.22035

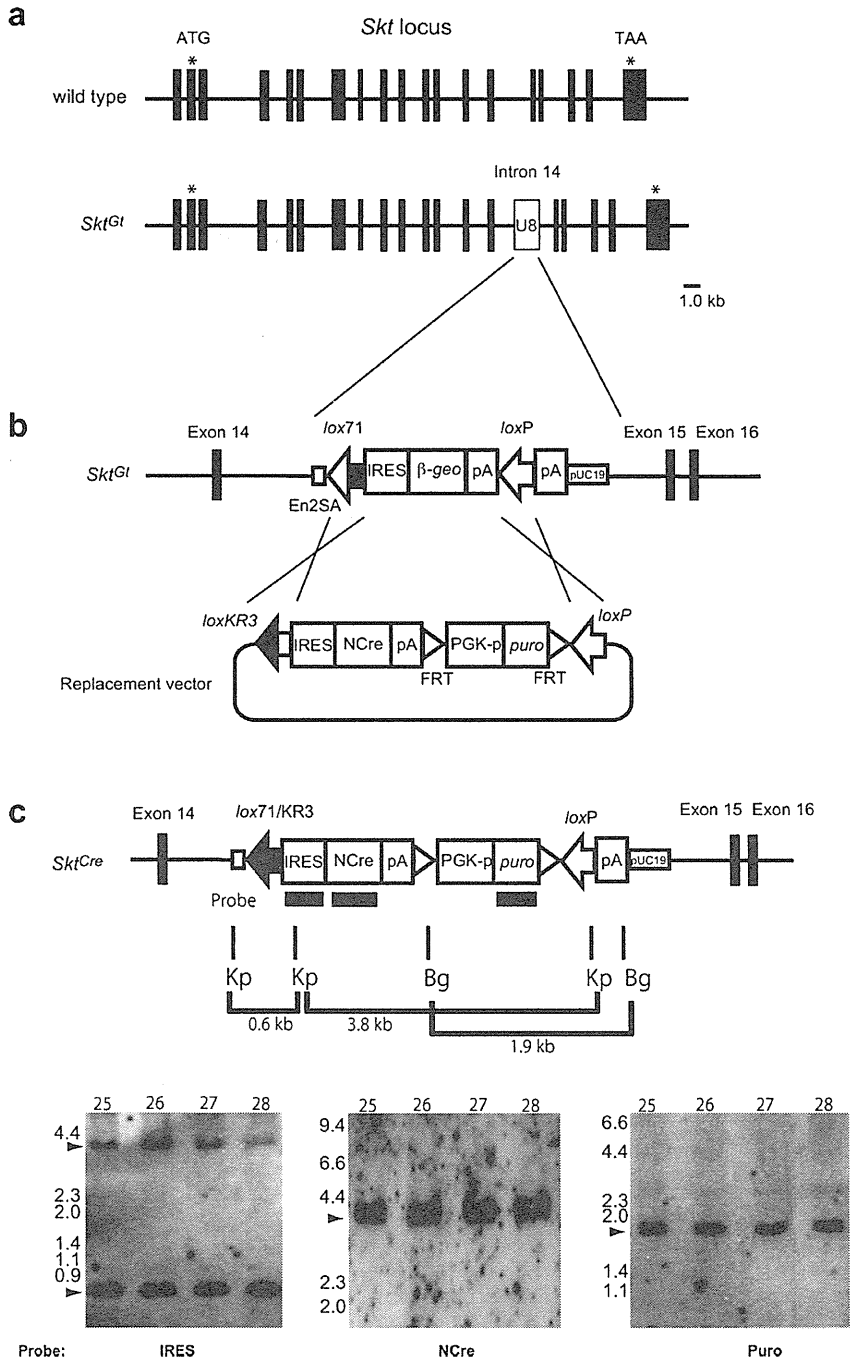

FIG. 1. Procedure for inserting a Cre-containing exchangeable cassette into the *Skt* locus. (**a**) The *Skt* gene consists of 19 exons and is located in the proximal region of chromosome 2. (**b**) In the Skt^{Gt} allele, the pU-Hachi (U8) trap vector, which is comprised of a mutated *lox*P (*lox*71), internal ribosomal entry site (IRES), β-*geo*, poly(A) sites, and *lox*P, is integrated into the 14th intron of the *Skt* gene. Replacement vector includes an exchange cassette, which contains another mutated *lox*P (*lox*KR3), IRES, Cre with nuclear-localization-signal sequences (NCre), poly(A) sites, a FRT-flanked puromycin resistance (*puro*) gene expression unit, and *lox*P. When the replacement vector is introduced into the Skt^{Gt} ES cells, specific recombination occur between *lox*71 and *lox*KR3. (**c**) In the Skt^{Cre} ES cells, U8 in Skt^{Gt} genome is replaced by the exchange cassette. To confirm the correct targeting event, genomic DNA of the survived ES clones digested with Kpn I (Kp) or Bgl II (Bg) was subjected to Southern blot analysis. The DNA fragments corresponding to IRES, Cre, and *puro* were used as probes for hybridization. All loaded samples (#25, #26, #27, and #28) exhibit the correct targeting event, judged by detection of the expected bands in each blot (arrowheads).

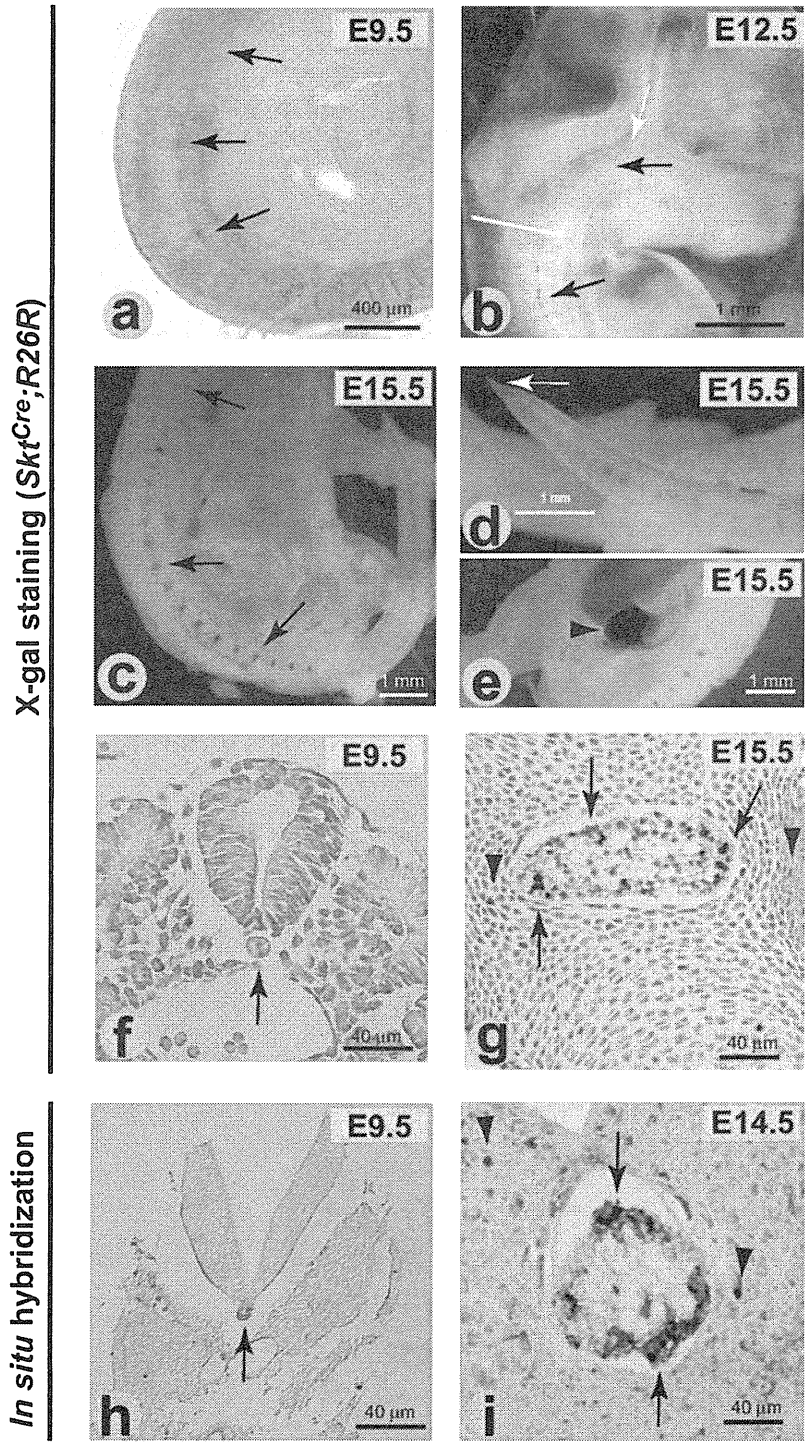

FIG. 2. Cre-mediated recombination in Skt^{Cre}; R26R embryos and in situ hybridization for *Skt* mRNA during embryognesis. Whole-mount X-gal staining of E9.5 (**a**) and E12.5 (**b**) Skt^{Cre}; R26R embryos. Black arrows indicate β-galactosidase (β-gal) activity at the region corresponding to the notochord. A white arrow and line in (**b**) represent the anterior end of the notochord and the first somite border, respectively. (**c–e**) Whole-mount X-gal staining in E15.5 Skt^{Cre}; R26R embryos. Black arrows indicate positive staining in the nucleus pulposus (NP). A white arrow in (d) represents the posterior end of the notochord. β-gal activity was also detected in the mesonephros (e, arrowhead). (**f**) Transverse sections of E9.5 Skt^{Cre}; R26R embryos and (*g*) sagittal sections of the vertebral region in E15.5 Skt^{Cre}; R26R embryos. Arrows indicate β-gal-positive cells located in the notochord and NP. Note that β-gal-positive cells are also observed in the annulus fibrosus (AF) (g, arrowheads). (**h**,**i**) In situ hybridization using an antisense probe for *Skt*. The *Skt* messages were detected in the notochord of E 9.5 embryos (h, arrow). In E14.5 embryos, the *Skt* transcripts were localized in the region corresponding to the NP (i, arrows) and a portion of AF cells (i, arrowheads).

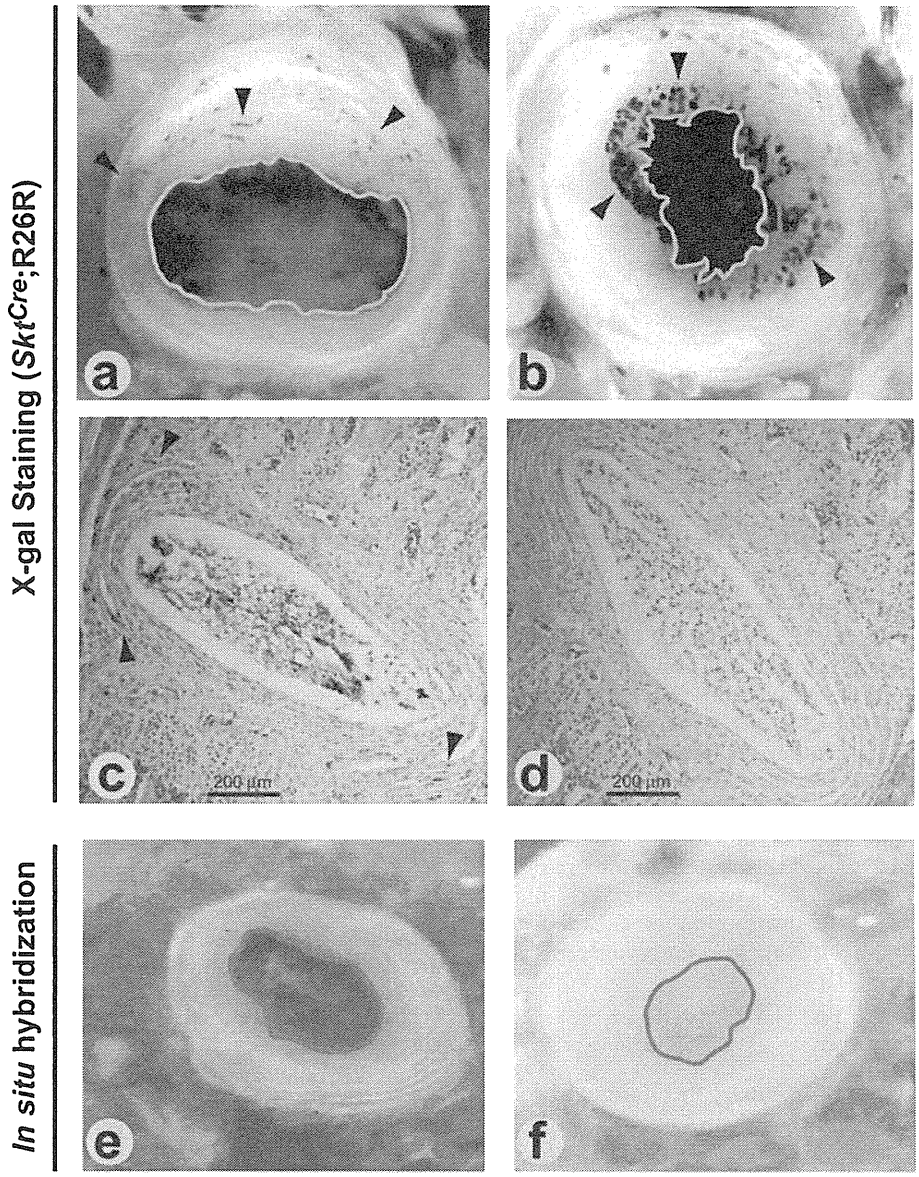

FIG. 3. Cre-mediated recombination in the adult Skt^{Cre}; R26R intervertebral discs (IVD) and whole mount in situ hybridization of adult IVD for *Skt* mRNA. Transversal views of the X-gal stained lumbar (**a**) and caudal (**b**) IVD in Skt^{Cre}; R26R mice are shown. The nucleus pulposus (NP) the enclosed by a gray line is intensively stained as β-galactosidase (β-gal)-positive. Note that β-gal activity was also detected in the annulus fibrosus (AF) (arrowheads). (**c**) Transverse sections of the caudal IVD indicated in (b) show β-gal activity in the NP and sparsely in the AF (arrowheads). (**d**) No X-gal staining was detected in the caudal IVD in wild type mice. (**e**) In situ hybridization using an antisense *Skt* probe demonstrates the positive purple staining in the NP enclosed by a gray line, but no staining in the AF (outside the gray line). (**f**) No hybridization signals were detected using the sense *Skt* probe.

are expressed in the notochord starting from E9.5 or earlier, and in the NP. However, the *P0* and *Shh* promoters are also active in other contiguous tissues along the midline (e.g., *P0*: neural crest and dorsal root ganglion, *Shh*: floor plate). Because these tissues may affect the notochord and/or its derivatives in development, complication in phenotype interpretation of the conditional alleles is predicted.

The *Sickle tail*^{GtAyu80211MEG} (Skt^{Gt}) strain was established in our gene trap insertional mutagenesis screen (Araki *et al.*, 2009; Semba *et al.*, 2006). In Skt^{Gt} embryos, the β-*geo* reporter within the trap vector is

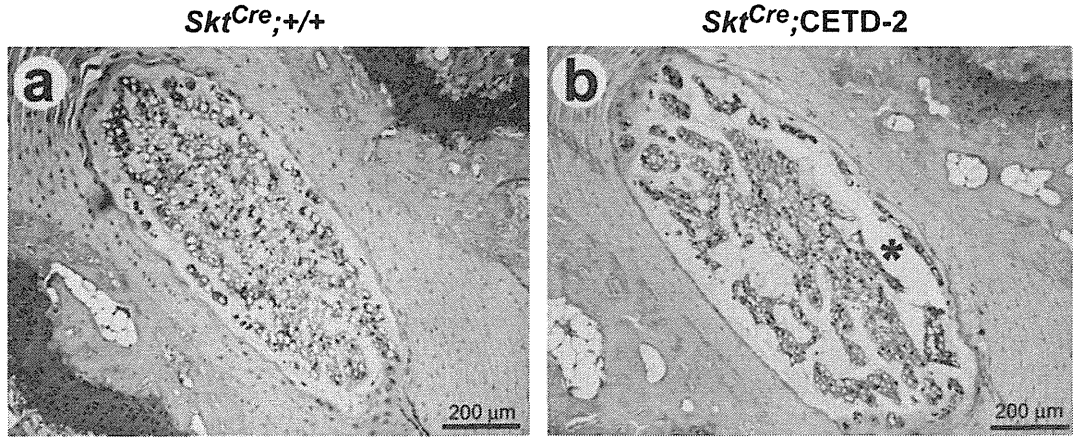

FIG. 4. Histological analysis of the caudal intervertebral discs (IVD) in Skt^{Cre}; CETD-2 mice aged 8 weeks. Transverse sections of the caudal IVD of Skt^{Cre}; +/+ (**a**) and Skt^{Cre}; CETD-2 mice (**b**) were stained with Safranin O, red staining for the cartilage and nucleus pulposus (NP), and with Fast green, counter staining. Safranin O staining identifies proteoglycans in the extracellular matrix of NP cells. Note that a marked reduction of the Safranin O-positive NP areas is detected in the Skt^{Cre}; CETD-2 IVD (b). Asterisk indicates a hollow cavity observed in the Skt^{Cre}; CETD-2 NP.

strongly expressed in the notochord, NP, and mesonephros (Ando *et al.*, 2011; Semba *et al.*, 2006). Heterozygous Skt^{Gt} mice are normal, and homozygotes show mild kinky tails, but no abnormality in kidneys (derivatives of the mesonephros) and fertility. The trapped gene, *Skt*, encodes a protein containing a proline-rich region and a coiled-coil domain. Previously, we developed an exchangeable gene trap system using left element/right element (LE/RE) mutant *lox* sites (Araki *et al.*, 2010). We have used this system to integrate Cre recombinase into the *Skt* locus to generate Skt^{Cre} mice. Here, we analyze tissue distribution of Cre-mediated recombination by the Skt^{Cre} allele in embryogenesis and IVD development.

RESULTS

Generation of the Skt^{Cre} Line by Exchangeable Gene Trap

To generate Skt^{Cre} mice, we used an exchangeable gene trap system with Skt^{Gt} ES cells. In the Skt^{Gt} genome, the pU-Hachi (U8) gene trap vector is integrated into the 14th intron of the *Skt* gene on chromosome 2 (Semba *et al.*, 2006)(Fig. 1a). We used an exchange cassette containing IRES (internal ribosomal entry site)-NCre (nuclear-localization-signal Cre recombinase) to replace the IRES-β-*geo* (lacZ + neo^r)-pA unit in the Skt^{Gt} genome (Fig. 1b). Because IRES-β-*geo*-pA is flanked by a *lox*71 (RE mutant) site, the replacement vector was designed to have a *lox*KR3 (LE mutant) site (Fig. 1b). After co-electroporation of the replacement vector with pCAGGS-Cre (a Cre-expression vector), puromycin resistant colonies were picked and stocked. Subsequent Southern blot analysis revealed that 15 out of 24 clones were correctly replaced. We used restriction enzymes that cut both inside and outside of the replaced region. The correctly replaced clones showed a single band with expected size (Fig. 1c), representing neither random nor multiple integration. Thus, the Skt^{Cre} strain was established through chimeric mice production using them.

Characterization of Cre-Mediated Recombination

To monitor Cre-mediated recombination in tissues, Skt^{Cre} mice were bred with ROSA26 reporter (R26R) mice (Soriano, 1999). In R26R mice, Cre-mediated recombination activates lacZ expression driven by the ubiquitous ROSA26 promoter. Therefore, the β-galactosidase (β-gal) positive cells are regarded as Cre-expressing cells and their derivatives. We also performed in situ hybridization to compare β-gal activity with endogenous *Skt* expression.

In embryonic day (E) 9.5 Skt^{Cre};R26R embryos, β-gal activity was detected along the notochord (Fig. 2a). Transverse sections of the embryos showed β-gal positive cells were located in the notochord (Fig. 2f, arrow), but the notochord sheath was negative. No reporter activity was detected in E8.5 or earlier stage embryos (data not shown). In E12.5 embryos, β-gal activity was continuously observed in the notochord (Fig. 2b, black arrows), and notably reporter activity was detected at the anterior end of the notochord (Fig. 2b, white arrow). In E15.5, the IVD located between condensed cartilage primordium were stained as lacZ positive (Fig. 2c,f, arrows). β-gal-positive IVD are observed along the midline by the posterior end (Fig. 2d, white arrow). Although the lacZ positive cells were predominately localized in the NP, a small population of AF cells (outside the NP) was stained (Fig. 2g, arrowheads). At this stage, the mesonephros was also X-gal stained (Fig. 2e, arrowhead), similar to Skt^{Gt} embryos (Semba *et al.*, 2006). Besides IVD specificity, we found

that approximately 5% of total *Skt*^{Cre};R26R embryos show lacZ activity throughout the whole body (data not shown). To compare *Skt* mRNA localization, we performed in situ hybridization to sections of E9.5 and E14.5 embryos. As expected, *Skt* mRNA was localized in the notochord of E9.5 embryos (Fig. 2h, arrow). Although *Skt* mRNA was localized mainly in the NP of E14.5 embryos (Fig. 2i, arrows), *Skt* signals were also detected in the AF (Fig. 2i, arrowheads).

In adult *Skt*^{Cre};R26R mice, β-gal activity was detected in all IVD (Fig. 3a,b and data not shown). While the β-gal-positive populations were localized mainly in the NP (Fig. 3a,b, enclosed by a gray line), minor populations in the AF (outside the NP) were also positively stained (Fig. 3a,b, arrowheads). In contrast, whole mount in situ hybridization of adult IVD revealed that the *Skt* signals were present only inside the NP (Fig. 3e, enclosed by gray line), not in the AF.

Selective Ablation of NP Cells in *Skt*^{Cre};CETD-2 Mice

Next, we attempted to produce a novel model for IVD degeneration by using *Skt*^{Cre} and CETD-2 strains (Sato and Tanigawa, 2005). In CETD-2 transgenic mice, Cre-mediated recombination activates expression of diphtheria toxin A-chain (DT-A) and, thus, induces subsequent cell death. Therefore, it is expected that selective ablation of *Skt*-expressing cells in the IVD occurs in hemizygotes for both transgene (*Skt*^{Cre};CETD-2 mice). Because only 2 out of 58 offspring obtained from crosses between heterozygous *Skt*^{Cre} and CETD-2 mice were hemizygotes for both transgenes, it is expected that most of *Skt*^{Cre};CETD-2 mice could not survive over weaning. The survived animals showed neither gate abnormality nor behavior abnormality over sexual maturation. But when the caudal vertebral region of the survived *Skt*^{Cre};CETD-2 animals was examined histologically, a marked reduction of Safranin O-positive NP areas was observed (Fig. 4b). The details in lethality of the *Skt*^{Cre};CETD-2 mice will be described elsewhere.

DISCUSSION

In this study, we established a novel Cre knock-in mouse line, *Skt*^{Cre}, which expresses Cre recombinase under control of the *Skt* promoter. To establish *Skt*^{Cre}, we used the original *Skt*^{Gt} ES cell stock to exchange β-*geo* for *cre*. Thus, Cre expression in *Skt*^{Cre} embryos was identical to reporter expression in *Skt*^{Gt} embryos [Fig. 2a–d, (Semba *et al.*, 2006), and (Ando *et al.* 2011)]. Further, Cre-mediated recombination in *Skt*^{Cre};R26R mice is also identical to *Skt* mRNA expression in embryogenesis (Fig. 2e–h). Because *Skt* is also expressed in ES cells (Semba *et al.*, 2006), *Skt* is expected to be weakly expressed in the inner cell mass (ICM) of blastocysts. Therefore, it is likely that the small number of *Skt*^{Cre};R26R embryos showing ubiquitous reporter expression resulted from Cre-mediate recombination in the ICM. These results strongly suggest that Cre expression in *Skt*^{Cre} mice mimics reporter expression of *Skt*^{Gt} mice and endogenous *Skt* expression in embryogenesis.

When compared with other Cre-driver strains, *Skt*^{Cre} shows more specific activity in notochordal cells. In *shhcre* (Choi *et al.*, 2008), *Foxa2*^{iCre} (Uetzmann *et al.*, 2008), and Foxa2 NFP-Cre (Kumar *et al.*, 2007) mice, Cre is expressed in the notochord as well as many other contiguous tissues along the midline (such as the floor plate and embryonic endoderm). In Nodal PNC-Cre (Kumar *et al.*, 2007) and Noto-cre (McCann *et al.* 2012) mice, Cre expression is specific but restricted to the posterior notochord. As shown in Figure 2c (white arrows), Cre expression in *Skt*^{Cre} mice was detected in the anterior end of the notochord. Therefore, it is advantageous to use *Skt*^{Cre} mice for cell-lineage track or conditional knockout experiments particularly targeting to the whole notochord.

In adult *Skt*^{Cre};R26R IVD, Cre-mediated recombination was observed in the NP and sparsely in the AF. Our in situ hybridization experiments showed that *Skt* mRNA is expressed in the embryonic AF but not in the adult AF. Therefore, it is assumed that *Skt* is expressed transiently and sporadically in the embryonic AF. Because the NP and AF are notochord- and somite-derivatives (Smith *et al.*, 2011), respectively, it is interesting to analyze the precise regulation of *Skt* expression in IVD development. While *Skt*^{Cre} mice are not suitable for NP-specific conditional knockout experiments, they are useful for targeting broader areas of adult IVD.

Because of low genotype frequency, most of *Skt*^{Cre};CETD-2 mice are presumed to be lethal. However, the survived hemizygous animals for both transgenes showed a marked decrease in NP cells of the caudal vertebral region (Fig. 4). This morphological change in the *Skt*^{Cre};CETD-2 mice is thought to be the effects of DT-A expression in notochordal cells. Thus far, young animals look healthy and survive over sexal maturation, however, we have not ruled out degeneration of IVD in aged mice. Consequently, we generated the *Skt*^{Cre} strain useful for analyzing the processes in development and degeneration of mammalian IVD. Conditional knockout of the genes expressed in the IVD using the *Skt*^{Cre} or other Cre-drivers may contribute to molecular dissection of the mechanisms that govern life and death of IVD in humans.

MATERIALS AND METHODS

Exchangeable Gene Trap and Screening

The exchangeable gene trap method was carried out as described by Araki *et al.* (2009). We used the TT2 ES cells (Yagi *et al.*, 1993), and the details of cell culture conditions as well as screening conditions for targeting

events were described previously (Araki *et al.*, 1999, 2010). Twenty-four puromycine resistant colonies were picked up and expanded for genomic DNA extraction. Southern blot analysis was performed using the DIG non-radio active system (Roche Diagnostics Japan, Tokyo, Japan) according to the manufactures' instructions.

Generation of *Skt*^{Cre} Mice

For the production of *Skt*^{Cre} mice, ICR (CLEA Japan, Inc., Tokyo, Japan) morula embryos were used as hosts to obtain aggregation chimaeras with the positive ES clones (Nagy *et al.*, 2003). To obtain ES-derived heterozygous mice, the chimeras were bred with C57BL/6Jcl mice (CLEA Japan). The same strain was used for backcrossing to maintain the *Skt*^{Cre} strain. *Skt*^{Cre} mice were genotyped by using PCR primers for the Cre gene (5′-aat gct tct gtc cgt ttg cc-3′ and 5′-cta cac cag aga cgg aaa tc-3′). R26R mice (Soriano, 1999) were maintained by intercrossing between homozygous mice. CETD-2 transgenic mice (Sato and Tanigawa, 2005) were bred with *Skt*^{Cre} mice after at least 10 generations of inbreeding. CETD-2 mice were genotyped using PCR primers for the DT-A gene described in http://mgc.wustl.edu/Protocols/PCRGenotypingPrimerPairs/tabid/154/Default.aspx. *Skt*^{Cre} mice are available from CARD (Center for Animal Resources and Development, Kumamoto University, http://card.medic.kumamoto-u.ac.jp/) to the research community upon request. All experiments in this study were approved in advance by *the Animal Welfare Committees of Kumamoto University* and *Tokai University.*

Histochemical Staining and In Situ Hybridization

Whole-mount staining for lacZ activity was performed as described previously (Semba *et al.*, 2006). Following staining, tissues were refixed in 4% paraformaldehyde and washed with phosphate buffered saline (PBS) several times, then embedded in paraffin. For adult spine, tissues were decalcified by Morse's solution (10 % sodium citrate and 22.5% formic acid) before embedding. From 4 to 8-μm sections were counterstained with nuclear fast red (MERK, Tokyo, Japan). Chemical reagents were purchased from Nakalai tesque (Kyoto, Japan). In situ hybridization was performed as described previously (Taniguchi *et al.*, 2011). For the *Skt* cDNA Probe, a 711-bp PCR fragment spanning exon 3 to exon 7 was cloned into pGEM-T Easy vector (Promega, Tokyo, Japan). The Spe I and Nco I digests were used as templates for synthesis of antisense and sense RNA probes, respectively.

ACKNOWLEDGMENTS

The authors thank Mses. Kumiko Ishikawa and Masami Yaguchi for their excellent technical assistant. They also thank Ms. Yoko Kameyama and Mr. Hideaki Hasegawa, the Education and Research Support Center, Tokai University, for their technical support on histology. They are grateful for contribution of Dr. Kenji Imai to experimental design in the early phase of the project.

LITERATURE CITED

Ando T, Semba K, Suda H, Sei A, Mizuta H, Araki M, Abe K, Imai K, Nakagata N, Araki K, Yamamura K. 2011. The floor plate is sufficient for development of the sclerotome and spine without the notochord. Mech Dev 128:129-140.

Araki M, Araki K, Yamamura K. 2009. International gene trap project: Towards gene-driven saturation mutagenesis in mice. Curr Pharm Biotechnol 10:221-229.

Araki K, Imaizumi T, Sekimoto T, Yoshinobu K, Yoshimuta J, Akizuki M, Miura K, Araki M, Yamamura K. 1999. Exchangeable gene trap using the Cre/mutated lox system. Cell Mol Biol (Noisy-le-grand) 45:737-750.

Araki K, Okada Y, Araki M, Yamamura K. 2010. Comparative analysis of right element mutant lox sites on recombination efficiency in embryonic stem cells. BMC Biotechnol 10:29.

Choi KS, Cohn MJ, Harfe BD. 2008. Identification of nucleus pulposus precursor cells and notochordal remnants in the mouse: Implications for disk degeneration and chordoma formation. Dev Dyn 237:3953-3958.

Christ B, Huang R, Scaal M. 2004. Formation and differentiation of the avian sclerotome. Anat Embryol (Berl) 208:333-350.

Freemont AJ. 2009. The cellular pathobiology of the degenerate intervertebral disc and discogenic back pain. Rheumatology (Oxford) 48:5-10.

Kumar A, Yamaguchi T, Sharma P, Kuehn MR. 2007. Transgenic mouse lines expressing Cre recombinase specifically in posterior notochord and notochord. Genesis 45:729-736.

McCann MR, Tamplin OJ, Rossant J, Seguin CA. 2012. Tracing notochord-derived cells using a Noto-cre mouse: Implications for intervertebral disc development. Dis Model Mech 5:73-82.

Nagy A. 2000. Cre recombinase: The universal reagent for genome tailoring. Genesis 26:99-109.

Nagy A, Gertsenstein M, Vintersten K, Behringer R. 2003. Manipulating the mouse embryo, 3rd ed. New York: Cold Spring Harbor Laboratory Press.

Risbud MV, Schaer TP, Shapiro IM. 2010. Toward an understanding of the role of notochordal cells in the adult intervertebral disc: From discord to accord. Dev Dyn 239:2141-2148.

Saga Y, Takeda H. 2001. The making of the somite: Molecular events in vertebrate segmentation. Nat Rev Genet 2:835-845.

Sakai D. 2008. Future perspectives of cell-based therapy for intervertebral disc disease. Eur Spine J 17 (Suppl 4):452-458.

Sato M, Tanigawa M. 2005. Production of CETD transgenic mouse line allowing ablation of any type of specific cell population. Mol Reprod Dev 72:54-67.

Semba K, Araki K, Li Z, Matsumoto K, Suzuki M, Nakagata N, Takagi K, Takeya M, Yoshinobu K, Araki M, Imai K, Abe K, Yamamura K. 2006. A novel murine gene, Sickle tail, linked to the Danforth's short tail locus, is required for normal development of the intervertebral disc. Genetics 172:445-456.

Smith LJ, Nerurkar NL, Choi KS, Harfe BD, Elliott DM. 2011. Degeneration and regeneration of the intervertebral disc: Lessons from development. Dis Model Mech 4:31-41.

Soriano P. 1999. Generalized lacZ expression with the ROSA26 Cre reporter strain. Nat Genet 21:70-71.

Stemple DL. 2005. Structure and function of the notochord: an essential organ for chordate development. Development 132:2503-2512.

Taniguchi Y, Tanaka O, Sekiguchi M, Takekoshi S, Tsukamoto H, Kimura M, Imai K, Inoko H. 2011. Enforced expression of the transcription factor HOXD3 under the control of the Wnt1 regulatory element modulates cell adhesion properties in the developing mouse neural tube. J Anat 219:589-600.

Uetzmann L, Burtscher I, Lickert H. 2008. A mouse line expressing Foxa2-driven Cre recombinase in node, notochord, floorplate, and endoderm. Genesis 46:515-522.

Walmsley R. 1953. The development and growth of the intervertebral disc. Edinb Med J 60:341-364.

Yagi T, Tokunaga T, Furuta Y, Nada S, Yoshida M, Tsukada T, Saga Y, Takeda N, Ikawa Y, Aizawa S. 1993. A novel ES cell line, TT2, with high germline-differentiating potency. Anal Biochem 214:70-76.

Yamauchi Y, Abe K, Mantani A, Hitoshi Y, Suzuki M, Osuzu F, Kuratani S, Yamamura K. 1999. A novel transgenic technique that allows specific marking of the neural crest cell lineage in mice. Dev Biol 212:191-203.